Mathematical Models and Methods in Applied Sciences
Vol. 23, No. 7 (2013) 1177–1215

DOI: 10.1142/S0218202513500061

SIMULATIONS OF THE LIFSHITZ–SLYOZOV EQUATIONS: THE ROLE OF COAGULATION TERMS IN THE ASYMPTOTIC BEHAVIOR

THIERRY GOUDON
Team COFFEE, INRIA Sophia Antipolis, Méditerrannée and Labo. J. A. Dieudonné, UMR 7351 CNRS — Université Nice Sophia Antipolis, Parc Valrose, F-06108 Nice, France
thierry.goudon@inria.fr

FRÉDÉRIC LAGOUTIÈRE*
Département de Mathématiques, Faculté des Sciences d'Orsay, Université Paris-Sud 11 Bâtiment 425, F-91405 Orsay Cedex, France
frederic.lagoutiere@math.u-psud.fr

LÉON MATAR TINE
UMR 8145 CNRS — Université Paris V — Paris Descartes, 45 Rue des Saint-Pères, Paris, France
Laboratoire d'Analyse Numérique et d'Informatique (LANI), Université Gaston Berger, B. P. 234 Saint-Louis, Sénégal

Received 20 March 2012
Revised 27 May 2012
Accepted 4 June 2012
Published 16 November 2012
Communicated by E. Zuazua

We consider the Lifshitz–Slyozov system that describes the kinetics of precipitation from supersaturated solid solutions. We design specific Finite Volume schemes and we investigate numerically the behavior of the solutions, in particular the large time asymptotics. Our purpose is two-fold: first, we introduce an adapted scheme based on downwinding techniques in order to reduce the numerical diffusion; second, we discuss the influence of coagulation effects on the selection of the asymptotic profile.

Keywords: Lifshitz–Slyozov equation; large time asymptotic behavior; anti-dissipative Finite Volume algorithm; coagulation terms.

AMS Subject Classification: 65M08, 65R20, 82C05, 35L60, 45K05, 82D60, 82C26

*Corresponding author

1. Introduction

The Lifshitz–Slyozov system models the formation of grains in supersaturated solid solutions. The dynamics can be thought of as an interaction between macroparticles and monomers. The particles are described by their size-density $f(t,x)$, where the variable $x \geq 0$ is interpreted as the volume of the particle; the monomers are described by their density $c(t)$. The evolution of the solution is governed by addition to or removal from clusters of monomers. We denote by $a(x) \geq 0$ and $b(x) \geq 0$ respectively, the rates characterizing these phenomena. Accordingly the density f obeys the following transport equation

$$\begin{cases} \partial_t f + \partial_x(Vf) = 0, & t \geq 0, \ \ x \geq 0, \\ V(t,x) = a(x)c(t) - b(x), \end{cases} \tag{1.1}$$

associated with a non-negative initial value $f(0,x)$. It is coupled to the integral equation

$$c(t) + \int_0^\infty x f(t,x)\mathrm{d}x = \rho, \quad t \geq 0, \tag{1.2}$$

which determines the monomers concentration $c(t)$ (the initial values are also assumed to satisfy $c(0) = \rho - \int_0^\infty x f(0,x)\mathrm{d}x \geq 0$). This relation is interpreted as a constraint of mass conservation. Indeed, $\int_0^\infty x f(t,x)\mathrm{d}x$ is (proportional to) the mass of material contained in the grains, thus adding $c(t)$, which is (proportional to) the mass of monomers, we obtain the total mass which remains constant. The dynamics depends on the precise dependence of the coefficients a, b with respect to the variable size. All the physics of the precipitation/dissolution process is embodied into these coefficients. Considering that mass transfer is driven by monomers diffusion, we obtain

$$a(x) = x^{1/3}, \quad b(x) = 1. \tag{1.3}$$

For details on the model, we refer to the seminal paper of Lifshitz and Slyozov.[25] Further comments can be found in the treatise[19] or in Ref. 37. More recently, this model has been derived from mean-field theory and homogenization arguments.[28] A derivation from the Becker–Döring system, a discrete model of coagulation–fragmentation, is proposed in Ref. 7. We point out immediately two key features of the model:

- First, the rate of growth at $x = 0$, that is $a(0)c(t) - b(0)$, is naturally negative. Hence, neglecting any difficulty associated to the lack of regularity of the coefficients, the characteristics associated to $V(t,x)$ are outgoing on the boundary $x = 0$, which explains that we do not need a boundary condition.
- At any time, there exists a unique critical size $x_{\mathrm{crit}}(t)$ where the growth rate changes sign. More precisely, any grain with size $0 \leq x \leq x_{\mathrm{crit}}(t)$ shrinks, while grains larger than x_{crit} grow. This phenomenon where large grains are growing at the expense of the smaller ones is known as Ostwald ripening. For (1.3), we have $x_{\mathrm{crit}}(t) = 1/c(t)^3$.

The system (1.1)–(1.3) together with non-negative initial conditions has been mathematically investigated, and we refer to the developments in Refs. 6, 20, 30, 32 for the existence theory in various functional frameworks. It turns out that the question of the large time behavior of the solutions, which is of central importance in physical chemistry, is highly intriguing and challenging. Based on physical arguments, the following conclusions have been proposed in Ref. 25: as t goes to infinity,

- $c(t)$ tends to 0 and behaves like $K_{\rm LS}t^{-1/3}$, where $K_{\rm LS} > 0$ is a universal constant.
- The total number of macroparticles $M_0(t) = \int_0^\infty f(t,x)\mathrm{d}x$ behaves like $C_{\rm LS}t^{-1}$ where $C_{\rm LS}$ depends on $K_{\rm LS}$ and ρ.
- The mean radius of the particles

$$R_{\rm mean}(t) = \frac{1}{M_0(t)}\int_0^\infty x^{1/3} f(t,x)\mathrm{d}x$$

  goes to $+\infty$ like $t^{1/3}/K_{\rm LS}$.
- The solution $f(t,x)$ behaves like a rescaled universal asymptotic profile, which we denote by $M_{K_{\rm LS}}$.

The analysis of the problem has motivated a series of papers.[2,8,31,29] It turns out that the asymptotic behavior is much more rich and complicated. Investigating the large time behavior relies on the self-similarity properties of the equation. We can exhibit a one-parameter family of self-similar solutions: the parameter, which we denote by K, characterizes the size of the support of the self-similar solution and its regularity. The LS profile corresponds to the unique infinitely smooth profile, which is also the solution with the largest support. The other solutions are infinitely smooth, but at the tip of their support where they behave as a power law. Hence we address the question of the selection of the asymptotic profile among the members of this family. The — highly surprising — answer is that the selected profile depends on the initial data, and more precisely on its shape at the end of its support. The analysis of this unusual selection process is very intricate and suitable notions of stability need to be introduced. The influence of the tail of the initial data is pointed out in Refs. 1 and 26 and we refer to Refs. 31 and 29 for a sharp mathematical analysis of these phenomena. The numerical investigation proposed in Ref. 3 brings out the strange selection process. Furthermore, it also shows that the problem is highly challenging for numerics since fronts have to be preserved with accuracy on a long time range and spurious smoothing effects should be eliminated to preserve the correct asymptotic profile. Let us point out that the question is relevant for instance in metallurgy engineering where the design of certain alloys production processes are based on the Lifshitz–Slyozov predictions. Lifshitz–Slyozov's claim is also subject to controversy for experimentalists and quite recent micro-gravity investigations bring out the need of further analysis of the model.[36]

Before detailing the aims and scopes of the present paper, it is worth mentioning that several modifications of the system (1.1)–(1.3) have been introduced

in order to restore a more standard large time behavior. An interesting attempt consists in introducing diffusive corrections, derived from a discrete-to-continuous regime: we expect with such a reasoning to recover a behavior similar to what is known for the Becker–Döring system. This viewpoint is discussed, among others, in Refs. 10, 15, 7, 9, 35, 27, 23. Going back to a more microscopic description and the mean-field derivation of the Lifshitz–Slyozov system, it can be shown that fluctuations of the particles distribution can also lead to diffusive corrections, as detailed in Ref. 34. A different approach has been discussed in Ref. 25 of Sec. 3: since the precipitation/dissolution process produces larger and larger grains, the modeling assumption that the distance between clusters remains large so that they do not interact directly becomes questionable as time becomes large. Accordingly, encounters between particles should be taken into account and (1.1) is replaced by

$$\partial_t f + \partial_x(Vf) = \lambda Q_{\rm coag}(f), \tag{1.4}$$

where $\lambda > 0$ and the coagulation operator $Q_{\rm coag}(f)$ is given by

$$\begin{aligned} Q_{\rm coag}(f)(t,x) &= \frac{1}{2}\int_0^x f(t,x-y)f(t,y)\mathrm{d}y - \int_0^\infty f(t,x)f(t,y)\mathrm{d}y \\ &= Q^+_{\rm coag}(f) - Q^-_{\rm coag}(f). \end{aligned} \tag{1.5}$$

The gain term $Q^+_{\rm coag}(f)$ characterizes the gain of particles with size x produced by the coalescence of particles with size $0 \le y \le x$ and $x-y$; the loss term $Q^-_{\rm coag}(f)$ characterizes the loss of particles with size x due to the collisions of such a particle x and another grain having size $y \ge 0$. The operator $Q_{\rm coag}$ satisfies the following mass conservation property:

$$\int_0^\infty x Q_{\rm coag}(f)\mathrm{d}x = 0,$$

while it implies a decay of the total number of particles since

$$\int_0^\infty Q_{\rm coag}(f)(t,x)\mathrm{d}x \le 0.$$

As far as we are concerned with existence issues, the analysis of the modified model is discussed in Refs. 5 and 21. From the discussion in Ref. 25, where the family of self-similar solutions is already identified, it is expected that the collision term induces a selection process which in turn, in the limit of vanishing λ, makes the LS profile the most physically relevant. A breakthrough in this direction is due to Ref. 17 where the existence of a stationary solution for the model with collision is proved. The obtained solution decays exponentially fast and it is isolated in a suitable functional space. In this paper the question we address is two-fold.

- As pointed out in Ref. 3, capturing the correct asymptotic profile is numerically challenging: numerical diffusion smoothes out the fronts so that we can be artificially led to the LS profile. We also refer to the conclusions of the sharp investigations in Ref. 4. The investigation of the coagulation-free problem in Ref. 3

uses the WENO scheme, see Refs. 18 and 38, but for sharp profiles the problem is very stiff and the computational cost is high. On the other hand, a specific Finite Volume scheme is introduced in Ref. 13, but even if the scheme has nice analytical properties, it is not able to capture non-smooth profiles (see results and comments in Ref. 13 of Sec. 5). Therefore, we wish to design a specific scheme, with reduced numerical diffusion. Our approach is based on an adaptation of downwinding techniques, as developed in Ref. 11.

- In the same spirit as in Ref. 3, we wish to discuss on numerical grounds the effect of the coagulation term Q_{coag}. The method we propose relies on a time-splitting where we first solve the transport part of the equation, and second the collisional part. To this end, we tested several methods to evaluate the collision operator. This revealed that it is performing to make use of the conservative Finite Volume method presented in Ref. 14.

The paper is organized as follows. In Sec. 2 we collect some basic material about the Lifshitz–Slyozov model. In particular, we describe a relevant rescaling of the equation and remind the derivation of the self-similar profiles. Section 3 is devoted to the presentation of the numerical scheme for (1.1)–(1.3). In contrast to the WENO scheme, which is a high-order reconstruction flux method for the advection equation, we introduce a first-order (explicit) scheme. However, the construction relies on an anti-dissipative approach which eliminates numerical diffusion and, in turn, we will be able to confirm the results of Ref. 3 for a reduced computational cost. We detail in Sec. 4 possible treatments of the coagulation operators, paying attention to the incorporation of the Finite Volume approach of Ref. 14 in our scheme for the Lifshitz–Slyozov model.

2. Basic Results

Let us start with a few remarks concerning the model (1.2)–(1.5). We shall perform here some formal manipulations in order to bring out interesting properties. Due to the singularity of the kinetic coefficients at $x = 0$, the justification of these relations might need some technicalities, see Refs. 5, 8 and 20. Firstly, since $V(t, 0) \leq 0$ and $\int_0^\infty Q_{\mathrm{coag}}(f)\mathrm{d}x \leq 0$, we have

$$\frac{\mathrm{d}}{\mathrm{d}t}\int_0^\infty f(t,x)\mathrm{d}x = -\int_0^\infty \partial_x(Vf)(t,x)\mathrm{d}x + \lambda\int_0^\infty Q_{\mathrm{coag}}(f)(t,x)\mathrm{d}x \leq 0.$$

Hence the total number of macroparticles is non-increasing. Secondly, for the evolution of the monomers concentration, we have

$$\begin{aligned}\frac{\mathrm{d}}{\mathrm{d}t}c(t) &= -\int_0^\infty V(t,x)f(t,x)\mathrm{d}x - \lambda\int_0^\infty xQ_{\mathrm{coag}}(f)(t,x)\mathrm{d}x \\ &= -\int_0^{x_{\mathrm{crit}}(t)} V(t,x)f(t,x)\mathrm{d}x - \int_{x_{\mathrm{crit}}(t)}^\infty V(t,x)f(t,x)\mathrm{d}x.\end{aligned}$$

Therefore $t \mapsto c(t)$ does not have *a priori* a monotone behavior. Nevertheless this relation shows that $c(t)$ remains positive for any time. Indeed if we assume the existence of $t_* > 0$ such that $c(t_*)$ vanishes, then the time derivative satisfies

$$\frac{\mathrm{d}}{\mathrm{d}t}c(t_*) = \int_0^\infty b(x)f(t_*,x)\mathrm{d}x > 0,$$

which leads to a contradiction. The final remark is concerned with a simplification of the model. As it is expected that the monomers concentration tends to 0, we replace, for large times, the mass conservation relation (1.2) by the constraint

$$\int_0^\infty xf(t,x)\mathrm{d}x = \rho.$$

Accordingly, in the growth rate, the definition of $c(t)$ is modified and we are finally led to consider the system

$$\begin{cases} \partial_t f + \partial_x(Vf) = \lambda Q_{\mathrm{coag}}(f), \\ V(t,x) = a(x)c(t) - b(x), \\ c(t) = \displaystyle\int_0^\infty b(x)f(t,x)\mathrm{d}x \left(\int_0^\infty a(x)f(t,x)\mathrm{d}x\right)^{-1}. \end{cases}$$

In the specific case of coefficients (1.3), $c(t)$ is nothing but the inverse of the mean radius. It is referred to as the Lifshitz–Slyozov–Wagner (LSW) model; it can be derived from the original model through suitable asymptotic arguments, see Ref. 22. This is the model dealt with in Refs. 30 and 2 (the last one with the simplification $a(x) = x$, $b(x) = 1$).

For discussing the large time behavior of the solutions of (1.1)–(1.3), or the model with coagulation (1.2)–(1.5), it is convenient to consider the following rescaling, see Ref. 3 and the references therein: we set

$$\begin{cases} f(t,x) = \dfrac{1}{(1+t)^2} g\left(\ln(1+t), \dfrac{x}{1+t}\right), \\ \tau = \ln(1+t), \quad y = \dfrac{x}{1+t}, \quad d(\tau) = (1+t)^{1/3}c(t). \end{cases}$$

As we shall see below, the rescaling is particularly important for numerics since it provides a natural way to reduce the computational domain. Indeed, since the dynamics tends to form infinitely large clusters as time becomes larger, we would need a huge computational domain to evaluate the behavior of the solution on a large time range. Accordingly, the computational resources needed for the simulation would become prohibitive. In rescaled variables, most of the information remains in a bounded domain. In rescaled variables the Lifshitz–Slyozov system

becomes

$$\begin{cases} \partial_\tau g(\tau,y) + \partial_y((y^{1/3}d(\tau) - 1 - y)g(\tau,y)) \\ \qquad = g(\tau,y) + \lambda Q^r_{\text{coag}}(g)(\tau,y) \quad \tau \geq 0, \ \ y \geq 0, \\ d(\tau)\exp\left(-\dfrac{\tau}{3}\right) + \displaystyle\int_0^\infty yg(\tau,y)\mathrm{d}y = \rho, \\ g(0,y) = g^0(y), \quad y \in \mathbb{R}_+, \quad d(0) = d^0. \end{cases} \tag{2.1}$$

The coagulation operator $Q^r_{\text{coag}}(g)$ reads

$$Q^r_{\text{coag}}(g)(\tau,y) = \frac{1}{2}\int_0^y g(\tau,y-u)g(\tau,u)\mathrm{d}u - \int_0^\infty g(\tau,y)g(\tau,u)\mathrm{d}u.$$

Notice that the homogeneity of the collision kernel is crucial in this manipulation (here we work with a constant collision kernel, but the reasoning applies for more general kernels as in Ref. 17). As a matter of fact, we still have the conservation property

$$\int_0^\infty yQ^r_{\text{coag}}(g)(\tau,y)\mathrm{d}y = 0.$$

As time tends to $+\infty$, we expect that $c(t)t^{1/3}$ tends to a constant $K > 0$; in other words

$$\lim_{\tau\to\infty} d(\tau) = K.$$

Accordingly, $d(\tau)\exp(-\tau/3) \sim K\exp(-\tau/3)$ becomes negligible for large rescaled times τ. We are thus led to the following rescaled version of the LSW equation, for $\tau \geq 0$, $y \geq 0$:

$$\begin{cases} \partial_\tau g + \partial_y(Wg) = g + \lambda Q^r_{\text{coag}}(g), \\ W(t,y) = Ky^{1/3} - 1 - y, \\ \displaystyle\int_0^\infty yg(\tau,y)\mathrm{d}y = \rho, \\ \displaystyle K = \int_0^\infty g(\tau,y)\mathrm{d}y\left(\int_0^\infty y^{1/3}g(\tau,y)\mathrm{d}y\right)^{-1}. \end{cases}$$

We are interested in stationary solutions, that is, we search for $y \mapsto M_K(y)$ verifying

$$\partial_y((y^{1/3}K - 1 - y)M_K) = M_K + \lambda\, Q^r_{\text{coag}}(M_K), \quad \int_0^\infty yM_K(y)\mathrm{d}y = \rho. \tag{2.2}$$

Equation (2.2) can be seen as an ODE with the term Q^r_{coag} as a perturbation.

Let us first discuss the coagulation-free equation

$$\partial_y((y^{1/3}K - 1 - y)M_K) = M_K.$$

We obtain

$$M_K(y) = -\frac{\mathrm{d}}{\mathrm{d}y}\left[\exp\left(\int_0^y \frac{\mathrm{d}\sigma}{\sigma^{1/3}K - 1 - \sigma}\right)\right]. \tag{2.3}$$

The question is now to identify parameters K that make the solution M_K admissible. The discussion relies on the properties of the function $T_K(z) = Kz - 1 - z^3$. We observe that $\frac{\mathrm{d}^2}{\mathrm{d}z^2}T_K(z) \leq 0$ for any $z \geq 0$; thus T_K is concave, and it reaches its maximum at $z = \sqrt{K/3}$: for any $z \geq 0$

$$T_K(z) \leq T_K^{\max} = 2\left(\frac{K}{3}\right)^{3/2} - 1.$$

The function $K \mapsto T_K^{\max}$ is increasing from $[0, +\infty[$ to $[-1, +\infty[$ and it vanishes at $K_{\mathrm{LS}} = \frac{3}{2^{2/3}}$. We are thus led to the following cases:

Case $K < K_{\mathrm{LS}}$. The solution M_K is not admissible since its first moment blows up. Indeed, noting $t_K(\sigma) = T_K(\sigma^{1/3})$, we have $t_K(\sigma) < 0$ for any $\sigma \geq 0$ and we remark that

$$(1+y)\exp\left(\int_0^y \frac{\mathrm{d}\sigma}{t_K(\sigma)}\right) = \exp\left(\int_0^y \frac{K\sigma^{1/3}\mathrm{d}\sigma}{(1+\sigma)(t_K(\sigma))}\right).$$

But $\frac{K\sigma^{1/3}d\sigma}{(1+\sigma)(t_K(\sigma))} \sim_{\sigma\to\infty} -K\sigma^{-5/3}$ which is integrable at infinity. Therefore,

$$\lim_{y\to+\infty}(1+y)\exp\left(\int_0^y \frac{\mathrm{d}\sigma}{t_K(\sigma)}\right) = l > 0$$

and we deduce that

$$yM_K(y) = \frac{y}{-t_K(y)}(1+y)\exp\left(\int_0^y \frac{\mathrm{d}\sigma}{t_K(\sigma)}\right)\frac{1}{1+y} \geq \frac{l}{4}\frac{1}{1+y}$$

holds for $y \geq Y > 0$ large enough. Consequently $yM_K(y) \notin L^1(\mathbb{R}_+)$ for $K < K_{\mathrm{LS}}$.

Case $K = K_{\mathrm{LS}}$. The point $z_0 = 2^{-1/3}$ is a double root of $T_{K_{\mathrm{LS}}}(z)$ and then we can write $T_{K_{\mathrm{LS}}}(z) = -(z - 2^{-1/3})^2(z + 2^{2/3})$. It allows to compute $M_{K_{\mathrm{LS}}}$: we arrive at

$$M_{K_{\mathrm{LS}}}(y) = \begin{cases} \dfrac{\exp\left(-\frac{(2y)^{1/3}}{1-(2y)^{1/3}}\right)}{(1-(2y)^{1/3})^{11/3}(1+1/2(2y)^{1/3})^{7/3}}, & 0 \leq y < y_0 = \dfrac{1}{2}, \\ 0, & y \geq y_0. \end{cases}$$

Case $K > K_{\mathrm{LS}}$**.** The polynomial $T_K(z)$ admits three distinct roots that we denote by z_-, z_0, z_+, with $z_- < 0 < z_0 < \sqrt{\frac{K}{3}} < z_+$. We set

$$\begin{cases} -T_K(z) = (z - z_0)(z - z_+)(z - z_-), \\ z_\pm = \dfrac{1}{2}(-z_0 \pm \sqrt{4K - 3z_0^2}), \\ p = \dfrac{3z_0^2}{(z_0 - z_-)(z_+ - z_0)}, \quad q = \dfrac{-3z_-^2}{(z_0 - z_-)(z_+ - z_-)}, \\ r = \dfrac{-3z_+^2}{(z_+ - z_0)(z_+ - z_-)} \end{cases}$$

and we are finally led to the following expression, see Ref. 3:

$$M_K(y) = \begin{cases} (y_0 y_- y_+)^{1/3} \dfrac{(1 - (y/y_0)^{1/3})^{p-1}}{(1 - (y/y_-)^{1/3})^{1-q}(1 - (y/y_+)^{1/3})^{1-r}}, & 0 \le y \le y_0 = \dfrac{1}{2}, \\ 0, & y > y_0, \end{cases}$$

with the relation

$$K = \frac{3(p+1)}{(2p+1)^{2/3} p^{1/3}}. \tag{2.4}$$

We plot in Fig. 1 the functions M_K corresponding to $K_{\mathrm{LS}} = 3/(2^{2/3})$ $(p = \infty)$, $K = 9 \times 7^{-2/3} \times 2^{-1/3} > K_{\mathrm{LS}}$ $(p = 2)$ and $K = 6 \times 5^{-2/3} > K_{\mathrm{LS}}$ $(p = 1)$. The profile $M_{K_{\mathrm{LS}}}$ is infinitely smooth, while the smaller K, the less regular the profile M_K. Similarly, letting K decrease will reduce the size of the support of the profile M_K.

Coming back to the evolution problem (1.1)–(1.3) we expect that

$$f(t,x) \sim_{t \to \infty} \frac{A_\rho}{(1+t)^2} \, M_K \left(\frac{x}{1+t} \right),$$

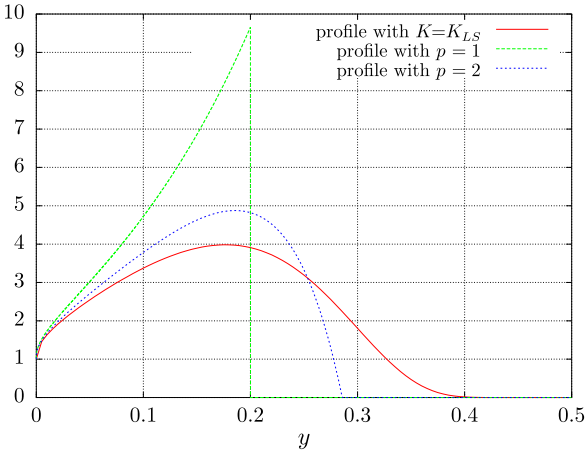

Fig. 1. Plot of asymptotic profiles M_K for $p = 1$, $p = 2$, $p = \infty$.

where $A_\rho = \rho(\int_0^\infty y M_K(y)\mathrm{d}y)^{-1}$ is a normalizing constant related to mass conservation. Of course, it remains to precise the selection of the parameter K in the asymptotic behavior. The conjecture of Lifshitz and Slyozov[25] is that the solution of (1.1)–(1.3) behaves for large time as the smooth profile $M_{K_{\mathrm{LS}}}$, whatever the shape of the initial data is. However, both numerical simulations[3] and mathematical analysis[29,31,33] have shown that the selection of the profile is much more amazing: considering a data with compact support, the large time behavior selects K according to the shape of the initial data at the tip of the support. Such a phenomenon is highly unusual and it has motivated the introduction of sharp notions to describe the behavior of a function at the end of its support, and for numerics it requires performing schemes with as reduced as possible numerical diffusion.

Of course, dealing with Eq. (2.2) containing the nonlinear collision term is certainly much more difficult. It could be quite natural to think of the solution as a fixed point of the mapping $\tilde{g} \mapsto g$, with g solution of

$$\partial_y((y^{1/3}K - 1 - y)g) = g + \lambda Q^r_{\mathrm{coag}}(\tilde{g}), \quad \int_0^\infty y g(y)\mathrm{d}y = \rho. \tag{2.5}$$

This iterative process is already described in Ref. 25. This viewpoint is further developed in Ref. 17 to prove the existence, for λ small enough, of a stationary solution close to $M_{K_{\mathrm{LS}}}$. Our goal here is to propose a numerical scheme to treat the Lifshitz–Slyozov equation with coagulation and to investigate numerically the influence of these encounters on the large time asymptotics.

What we observe based on the numerical simulations is the regularization effect of the collisions. Considering different initial data leading to different asymptotic profiles in the coagulation-free case, the numerical large time solutions become similar with collisions. Furthermore as the parameter λ in front of the coagulation operator tends to zero, the large time profile looks like the smooth $M_{K_{\mathrm{LS}}}$ profile. Of course further analysis will be necessary to decide whether this effect is due to the numerical approximation or really to the effect of encounters. However, the use of a specific non-dissipative scheme reduces the numerical diffusion, at least for the transport part, and the scheme is validated by performing simulation of the coagulation-free problem.

3. An Anti-Diffusive Finite Volume Scheme for the Lifshitz–Slyozov System

In this part we set up a new numerical scheme for the (collisionless) Lifshitz–Slyozov system (1.1)–(1.3). The scheme we propose is a Finite Volume scheme, with a flux reconstruction that cancels out the numerical diffusion. The method is first-order accurate, but in comparison to the fifth-order WENO scheme used in Ref. 3, it allows simulation of the solutions with a given accuracy for a reduced computational cost, and furthermore it allows to capture the large time behavior far beyond the capabilities of the WENO scheme. We point out again that reducing the numerical diffusion is crucial to capture the correct asymptotic profile. Even if

WENO is very efficient in preserving fronts, the problem becomes so stiff that the computations can be quite long when dealing with non-smooth data, as reported in Ref. 3. We start by describing how downwinding techniques taken from Ref. 11 apply for the conservative transport equation. Then, we detail the splitting scheme we use for solving (1.1)–(1.3). Finally, we compare numerical results with those obtained with the WENO scheme.

3.1. *A scheme for the transport equation*

In this section we are concerned with the simple transport equation

$$\partial_t f(t,x) + \partial_x (V(t,x) f(t,x)) = 0, \tag{3.1}$$

where $V(t,x)$ is a given smooth velocity field. We neglect any difficulties due to truncation of the computational domain, and we consider the problem set on $t \geq 0$, $x \geq 0$, assuming that $V(t,0) < 0$. We introduce a regular mesh, with constant step $\Delta x > 0$: the cells are the intervals $[x_{k-1/2}, x_{k+1/2}]$, $k \in \mathbb{N}$ with $x_{-1/2} = 0$, $x_{k+1/2} = (k+1)\Delta x$, and we denote by x_k the midpoint of the cell: $x_k = (k+1/2)\Delta x$. We denote by f_k^n the numerical unknown, which is intended to be an approximation of $\frac{1}{\Delta x}\int_{x_{k-1/2}}^{x_{k+1/2}} f(t^{(n)}, z)\mathrm{d}z$, where $t^{(0)} = 0 < t^{(1)} < \cdots < t^{(n)} < t^{(n+1)}$ defines a time-discretization, with possibly variable step $\Delta t^{(n)} = t^{(n+1)} - t^{(n)}$ in order to adapt to the time variation of V. We denote by V_k^n the approximation of the velocity *in* the cells (meaning that the approximation is piecewise constant) and by $V_{k-1/2}^n$ the velocity *at* the cell interfaces: namely, we set

$$\begin{aligned} V_k^n &= V(t^{(n)}, x_k), \qquad && n \in \mathbb{N},\ \ k \in \mathbb{N}, \\ V_{k-1/2}^n &= V(t^{(n)}, x_{k-1/2}), && n \in \mathbb{N},\ \ k \in \mathbb{N}. \end{aligned}$$

The scheme is defined by the relation

$$f_k^{n+1} = f_k^n - \frac{\Delta t^{(n)}}{\Delta x}(V_{k+1/2}^n f_{k+1/2}^n - V_{k-1/2}^n f_{k-1/2}^n). \tag{3.2}$$

It remains to define the interface fluxes $f_{k+1/2}^n$. When investigating the large time behavior of solutions to transport equations, one is faced to a classical drawback of usual stable schemes: numerical diffusion, in its general sense, that is, the deterioration of profiles, the spreading of the initial data and the loss of the dependence cone. High-order schemes (such as WENO...) are a cure, but are known to spread all the same the initial data, in *very* long time (what we are interested in here). On the other hand, the anti-diffusive, limited downwind scheme of Ref. 11, has the advantage of avoiding this spreading, keeping in arbitrary large time the profiles. Let us recall its basic principles in the case of advection with constant velocity. Arguing that the numerical diffusion process is due to the upwinding of the numerical fluxes, the idea is to take a downwind flux, the most downwind under some stability constraints. The stability constraints are those that lead to a local numerical maximum principle. We here propose to adapt this idea to the present problem.

The adaptation is devoted to treat the *conservative* advection equation with *non-constant* velocity. In this equation, the maximum principle is not satisfied in the same trivial sense, so that the stability constraints have to be modified. Another adaptation concerns a weaker property: the *positivity* of the solution.

Let us now go into details and describe precisely the scheme.

To define some correct stability criteria, it is convenient to rewrite (3.2) as follows:

$$f_k^{n+1} = f_k^n - \frac{\Delta t^{(n)}}{\Delta x} V_k^n (f_{k+1/2}^n - f_{k-1/2}^n) - \frac{\Delta t^{(n)}}{\Delta x} (f_{k+1/2}^n (V_{k+1/2}^n - V_k^n) + f_{k-1/2}^n (V_k^n - V_{k-1/2}^n)).$$

The last term is an approximation of $f\partial_x V(t^{(n)}, x_k)$ and the definition of the fluxes will be driven by anti-diffusive strategies for the advection equation

$$\partial_t f + V\partial_x f = 0. \tag{3.3}$$

We introduce the following notation:

- $\nu^n = \frac{\Delta t^{(n)}}{\Delta x}$.
- $m_{k+1/2}^n = \min(f_k^n, f_{k+1}^n)$, and $M_{k+1/2}^n = \max(f_k^n, f_{k+1}^n)$.
- If $V_k^n, V_{k+1/2}^n, V_{k-1/2}^n > 0$, then:

$$\begin{aligned} b_{k+1/2}^n &= \frac{1}{\nu^n V_k^n}(f_k^n - \max(f_k^n, f_{k-1}^n)) + \max(f_k^n, f_{k-1}^n) \\ &= \frac{1}{\nu^n V_k^n}(f_k^n - M_{k-1/2}^n) + M_{k-1/2}^n, \\ B_{k+1/2}^n &= \frac{1}{\nu^n V_k^n}(f_k^n - \min(f_k^n, f_{k-1}^n)) + \min(f_k^n, f_{k-1}^n) \\ &= \frac{1}{\nu^n V_k^n}(f_k^n - m_{k-1/2}^n) + m_{k-1/2}^n, \\ \mathscr{B}_{k+1/2}^n &= \begin{cases} \min\left(B_{k+1/2}^n, m_{k-1/2}^n \dfrac{V_{k-1/2}^n}{V_{k+1/2}^n} + \dfrac{f_k^n}{\nu^n V_{k+1/2}^n}\right), & \text{if } m_{k-1/2}^n \geq 0, \\ B_{k+1/2}^n, & \text{otherwise.} \end{cases} \end{aligned}$$

- If $V_k^n, V_{k+1/2}^n, V_{k-1/2}^n < 0$, then:

$$\begin{aligned} b_{k-1/2}^n &= \frac{1}{\nu^n |V_k^n|}(f_k^n - \max(f_k^n, f_{k+1}^n)) + \max(f_k^n, f_{k+1}^n) \\ &= \frac{1}{\nu^n |V_k^n|}(f_k^n - M_{k+1/2}^n) + M_{k+1/2}^n, \end{aligned}$$

$$B^n_{k-1/2} = \frac{1}{\nu^n |V^n_k|}(f^n_k - \min(f^n_k, f^n_{k+1})) + \min(f^n_k, f^n_{k+1})$$
$$= \frac{1}{\nu^n |V^n_k|}(f^n_k - m^n_{k+1/2}) + m^n_{k+1/2},$$
$$\mathscr{B}^n_{k-1/2} = \begin{cases} \min\left(B^n_{k-1/2}, m^n_{k+1/2}\dfrac{|V^n_{k+1/2}|}{|V^n_{k-1/2}|} + \dfrac{f^n_k}{\nu^n |V^n_{k-1/2}|}\right), & \text{if } m^n_{k+1/2} \geq 0, \\ B^n_{k-1/2}, & \text{otherwise.} \end{cases}$$

- If $V^n_k, V^n_{k+1/2}, V^n_{k-1/2}$ do not have the same sign, we set $b^n_{k+1/2} = \mathscr{B}^n_{k+1/2} = f^n_k$ if $V^n_{k+1/2} > 0$ and $b^n_{k+1/2} = \mathscr{B}^n_{k+1/2} = f^n_{k+1}$ if $V^n_{k+1/2} < 0$.
- $\mu^n_{k+1/2} = \max(m^n_{k+1/2}, b^n_{k+1/2})$ and $\mathscr{M}^n_{k+1/2} = \min(M^n_{k+1/2}, \mathscr{B}^n_{k+1/2})$.

The following statement makes the principles on which the construction of the fluxes is based clear.

Proposition 3.1. *We assume that the following standard Courant–Friedrichs–Levy (CFL) stability condition*:

$$\frac{\Delta t^{(n)}}{\Delta x} \max_k(|V^n_k|, |V^n_{k+1/2}|) \leq 1 \tag{3.4}$$

is satisfied. Then, for any k the set $[\mu^n_{k+1/2}, \mathscr{M}^n_{k+1/2}]$ is non-empty. Suppose that for any k the fluxes satisfy $f^n_{k+1/2} \in [\mu^n_{k+1/2}, \mathscr{M}^n_{k+1/2}]$. Then, the following assertions hold:

(i) *The scheme* (3.2) *is consistent with* (3.1).
(ii) *If $f^n_k \geq 0$ for any k then $f^{n+1}_k \geq 0$ too, if Δx is sufficiently small (otherwise a restricted CFL condition is requested to ensure the non-negativity*: $\Delta t^{(n)}/\Delta x \max_k(|V^n_{k+1/2}|) \leq 1/2$).
(iii) *Let us set*

$$f^{n\star}_k = f^n_k - \frac{\Delta t^{(n)}}{\Delta x} V^n_k (f^n_{k+1/2} - f^n_{k-1/2}), \quad k \in \mathbb{N}.$$

Let $j \in \mathbb{N}$. If $V^n_j \geq 0$ then $m^n_{j-1/2} \leq f^{n\star}_j \leq M^n_{j-1/2}$, while if $V^n_j \leq 0$ then $m^n_{j+1/2} \leq f^{n\star}_j \leq M^n_{j+1/2}$.

Proof. To discuss the properties of the scheme, we first suppose that $V^n_{k-1/2} > 0$, $V^n_k > 0$ and $V^n_{k+1/2} > 0$. Owing to (3.4), we have

$$\frac{1}{\nu^n V^n_k} - 1 \geq 0$$

and thus

$$\left(\frac{1}{\nu^n V^n_k} - 1\right)(f^n_k - \min(f^n_k, f^n_{k-1})) \geq 0.$$

It follows that

$$\frac{1}{\nu^n V_k^n}(f_k^n - \min(f_k^n, f_{k-1}^n)) + \min(f_k^n, f_{k-1}^n) \geq f_k^n. \tag{3.5}$$

On the same token, we have

$$\left(\frac{1}{\nu^n V_k^n} - 1\right)(f_k^n - \max(f_k^n, f_{k-1}^n)) \leq 0,$$

which leads to

$$\frac{1}{\nu^n V_k^n}(f_k^n - \max(f_k^n, f_{k-1}^n)) + \max(f_k^n, f_{k-1}^n) \leq f_k^n. \tag{3.6}$$

By definition $f_k^n \in [m_{k+1/2}^n, M_{k+1/2}^n]$ while (3.5) and (3.6) tell us $f_k^n \in [b_{k+1/2}^n, B_{k+1/2}^n]$. When $m_{k-1/2}^n \geq 0$, we also observe that (3.4) implies $m_{k-1/2}^n \frac{V_{k-1/2}^n}{V_{k+1/2}^n} + \frac{f_k^n}{\nu^n V_{k+1/2}^n} \geq \frac{f_k^n}{\nu^n V_{k+1/2}^n} \geq f_k^n$. Hence we have $f_k^n \in [b_{k+1/2}^n, \mathscr{B}_{k+1/2}^n]$. The argument adapts when V is locally negative (leading to $f_k^n \in [m_{k-1/2}^n, M_{k-1/2}^n] \cap [b_{k-1/2}^n, B_{k-1/2}^n]$) or changes sign (in which case the requirement $f_{k+1/2}^n \in [\mu_{k+1/2}^n, \mathscr{M}_{k+1/2}^n]$ implies that the scheme is the upwind scheme). The consistency of the scheme follows from the very definition of $m_{k+1/2}^n$ and $M_{k+1/2}^n$.

Let us now prove that f_k^{n+1} remains non-negative. The non-negativity $f_k^{n+1} \geq 0$ is equivalent to

$$\nu^n(V_{k+1/2}^n f_{k+1/2}^n - V_{k-1/2}^n f_{k-1/2}^n) \leq f_k^n.$$

Again, we start by assuming, for k fixed, $V_{k+1/2}^n, V_{k-1/2}^n, V_k^n > 0$. Then $f_k^{n+1} \geq 0$ is equivalent to

$$f_{k+1/2}^n \leq \frac{f_k^n}{\nu^n V_{k+1/2}^n} + f_{k-1/2}^n \frac{V_{k-1/2}^n}{V_{k+1/2}^n}.$$

Assuming $f_{k-1/2}^n \geq m_{k-1/2}^n$ yields the following sufficient condition for this relation to hold:

$$f_{k+1/2}^n \leq \frac{f_k^n}{\nu^n V_{k+1/2}^n} + m_{k-1/2}^n \frac{V_{k-1/2}^n}{V_{k+1/2}^n},$$

which justifies the definition of $\mathscr{B}_{k+1/2}^n$.

In the case $V_{k+1/2}^n, V_{k-1/2}^n, V_k^n < 0$ we obtain the following analog condition:

$$f_{k-1/2}^n \leq \frac{f_k^n}{-\nu^n V_{k-1/2}^n} + m_{k+1/2}^n \frac{-V_{k+1/2}^n}{-V_{k-1/2}^n}.$$

In the other cases we just choose the standard upwind flux, which is known to ensure the non-negativity *under the restricted CFL condition*

$$\frac{\Delta t^{(n)}}{\Delta x} \max_k(|V_{k+1/2}^n|) \leq \frac{1}{2}.$$

Let us analyze this case in detail. In the case where $V^n_{k+1/2} < 0$ and $V^n_{k-1/2} > 0$, the non-negativity of f^{n+1}_k is ensured without any condition on the time step. The only problematic case is when $V^n_{k+1/2} > 0$ and $V^n_{k-1/2} < 0$ (where the cell can be "emptied" from the two sides). In this case, choosing the upwind fluxes leads to

$$f^{n+1}_k = f^n_k \left(1 - \frac{\Delta t^{(n)}}{\Delta x}(V^n_{k+1/2} - V^n_{k-1/2})\right).$$

Thus the non-negativity condition is

$$\frac{\Delta t^{(n)}}{\Delta x}(V^n_{k+1/2} - V^n_{k-1/2}) \leq 1$$

(which explains the CFL condition restriction by a factor $1/2$ in general). But now, assume that the velocity is Lipschitz with coefficient L. Then one has $V^n_{k+1/2} - V^n_{k-1/2} \leq L\Delta x$ and a sufficient condition on the time step becomes

$$\Delta t^{(n)} \leq \frac{1}{L}.$$

Asymptotically when Δx tends to 0, this is automatically satisfied when the CFL condition of the proposition is satisfied, that is why we retain only this classical condition.

We finally turn to the proof of (iii) which relies on the discretization of the advection equation (3.3). The construction is taken out from Ref. 11 and is based on the requirements to preserve the L^∞-norm and to satisfy the total variation diminishing (TVD) property. We have already seen that, in the case $V^n_{k-1/2} > 0$, $V^n_k > 0$, $V^n_{k+1/2} > 0$,

$$f^n_k \in [m^n_{k+1/2}, M^n_{k+1/2}] \cap [b^n_{k+1/2}, B^n_{k+1/2}] \neq \emptyset.$$

Now, we require that the numerical flux $f^n_{k+1/2}$ fulfills the same constraints

$$\begin{cases} m^n_{k+1/2} \leq f^n_{k+1/2} \leq M^n_{k+1/2}, & \text{consistency constraint,} \\ b^n_{k+1/2} \leq f^n_{k+1/2} \leq B^n_{k+1/2}, & \text{stability constraint.} \end{cases} \tag{3.7}$$

Combining the stability constraint in (3.7) to the consistency constraint $m^n_{k-1/2} \leq f^n_{k-1/2} \leq M^n_{k-1/2}$ we obtain

$$\frac{1}{\nu^n V^n_k}(f^n_k - M^n_{k-1/2}) + f^n_{k-1/2} \leq f^n_{k+1/2} \leq \frac{1}{\nu^n V^n_k}(f^n_k - m^n_{k-1/2}) + f^n_{k-1/2}.$$

Therefore, we deduce that

$$m^n_{k-1/2} \leq f^{n\star}_k = f^n_k - \nu^n V^n_k (f^n_{k+1/2} - f^n_{k-1/2}) \leq M^n_{k-1/2} \tag{3.8}$$

holds. We conclude that the discrete solution satisfies the following maximum principle:

$$\begin{cases} \max_{k\in\mathbb{N}}(f_k^{n\star}) \le \max_{k\in\mathbb{N}}(f_k^n), \\ \min_{k\in\mathbb{N}}(f_k^{n\star}) \ge \min_{k\in\mathbb{N}}(f_k^n). \end{cases}$$

The TVD property is also insured, it follows from Le Roux and Harten's incremental analysis.[16,24] The same can be done when the velocity is negative or changes sign: this ends the proof. □

The point now consists in defining $f_{k+1/2}^n$ so that on the one hand, Proposition 3.1 holds, and on the other hand the numerical diffusion is as reduced as possible: to this end we adopt a *downwinding* approach. When $V_{k-1/2}^n > 0$, $V_k^n > 0$ and $V_{k+1/2}^n > 0$, we choose the closest value to f_{k+1}^n that fulfills the requirements of Proposition 3.1. Namely $f_{k+1/2}^n$ will be the solution of the following problem:

$$\begin{aligned} &\text{To minimize} \quad |f_{k+1/2}^n - f_{k+1}^n| \\ &\text{under the constraint} \quad f_{k+1/2}^n \in [\mu_{k+1/2}^n, \mathscr{M}_{k+1/2}^n]. \end{aligned}$$

This minimization problem leads to the following three cases (again assuming that $V_{k-1/2}^n > 0$, $V_k^n > 0$ and $V_{k+1/2}^n > 0$):

$$\begin{cases} f_{k+1/2}^n = \mu_{k+1/2}^n & \text{if} \quad f_{k+1}^n \le \mu_{k+1/2}^n, \\ f_{k+1/2}^n = f_{k+1}^n & \text{if} \quad \mu_{k+1/2}^n \le f_{k+1}^n \le \mathscr{M}_{k+1/2}^n, \\ f_{k+1/2}^n = \mathscr{M}_{k+1/2}^n & \text{if} \quad f_{k+1}^n \ge \mathscr{M}_{k+1/2}^n. \end{cases} \tag{3.9}$$

When the velocity is locally positive, we note that the stability constraint involves f_{k-1}^n and f_k^n that are only upwind values for $f_{k+1/2}^n$; it justifies the naming of downwind flux under upwind constraint.

3.2. *Simulation of* (1.1)–(1.3)

Let us explain the derivation of the anti-dissipative scheme for the conservative equation (1.1) based on the idea developed in Sec. 3.1 by using a time-splitting.

- First, we solve the transport equation (1.1). Here, we know the discrete density f_k^n and the concentration c^n, approximation of the average of $f(t^{(n)},\cdot)$ on the kth-cell and $c(t^{(n)})$. The concentration is assumed constant during the time step, and thus the velocity field $V(t,x)$ is replaced by the given quantity $x^{1/3}c^n - 1$. The equation has the form (3.1) and we apply the scheme designed in the previous section. It defines f^{n+1}. Note that by construction the solution is non-negative.

- Second, we update the monomers concentration by setting:

$$c^{n+1} = \rho - \Delta x \sum_{k\in\mathbb{N}} x_k f_k^{n+1}$$

(recall that x_k is defined as the center of the kth-cell: $x_k = (k + 1/2)\Delta x$ for any $k \in \mathbb{N}$).

In the algorithm, the time step $\Delta t^{(n)}$ is evaluated at each iteration, it is computed so that the scheme satisfies the CFL condition (3.4).

Simulations of the Lifshitz–Slyozov system: *Comparison with a fifth-order WENO scheme*. To validate the scheme, we compare the simulations with those in Ref. 3. The domain is $[0, 800]$ with 80 points by length unit. As an initial condition we set

$$\rho = 41,$$
$$f^0(x) = \begin{cases} 0.1, & \text{for } x \in [10, 30], \\ 0, & \text{otherwise.} \end{cases} \tag{3.10}$$

This is a characteristic function and the corresponding profile M_K is determined by $K = 6 \times 5^{-2/3}$ (i.e. $p = 1$, see Sec. 2). This is the hardest case dealt with in Ref. 3. We perform the simulation with a Courant number $\nu^n \max |V_k^n, V_{k+1/2}^n| = 1/2$ (the maximum of the velocities is actually computed on the domain $[0, 800]$). The scheme detailed above is referred to as ADM (anti-dissipative method) and we compare in Fig. 2 with results provided by the fifth-order WENO scheme developed and used in Ref. 3. The evolution of the monomers concentration is basically the same. However, the interesting point is the discrepancies observed at the final time $t = 2000$ in the particles distribution profile. At such a large time we observe the smearing in the WENO simulation, and numerical diffusion is sensible. By contrast, the ADM scheme preserves accurately the shape of the expected profile. Furthermore, while we use the same mesh size, of course, the ADM run is faster by a factor 3/4 than the WENO simulation. The smoothing effect is confirmed by

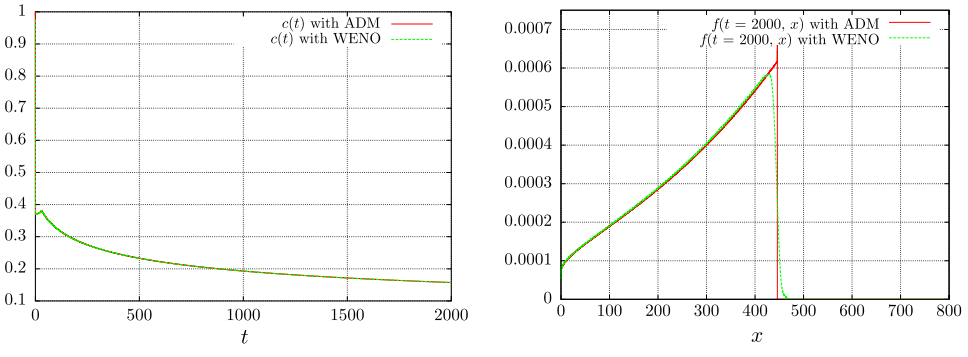

Fig. 2. Comparison of the WENO and the ADM schemes, with the data of Eq. (3.10). *Left*: evolution of the monomers concentration. *Right*: final solution at $t = 2000$.

the snapshots of the time evolution in Fig. 3: the numerical diffusion in the WENO simulation becomes visible after 1000 time units. The maximum is damped and the shape of the solution, in particular at the tip of the support, is smoothed. The effect increases as time grows.

3.3. *Simulation of the Lifshitz–Slyozov equation in rescaled variables*

As detailed in Sec. 2, in rescaled variables the Lifshitz–Slyozov system becomes

$$\begin{cases} \partial_\tau g(\tau,y) + \partial_y(W(\tau,y)g(\tau,y)) = g(\tau,y), & \tau \geq 0,\ \ y \geq 0, \\ W(\tau,y) = y^{1/3} d(\tau) - 1 - y, & \tau \geq 0,\ \ y \geq 0, \\ d(\tau)\exp(-\tau/3) + \displaystyle\int_0^\infty y g(\tau,y)\mathrm{d}y = \rho \text{ (constant)}, & \tau \geq 0, \\ g(0,y) = g^0(y), & y \geq 0. \end{cases}$$

The advantage now is that the solution is expected to converge for large τ to a compactly supported profile, while in original variables the mean radius goes to $+\infty$. Therefore, for the rescaled problem we considerably reduce difficulties related to the truncation of the computational domain. However, as remarked in Ref. 3, the price to be paid is to increase significantly the stiffness of the problem. In practice, it requires for the WENO scheme some restrictions on the CFL number to prevent the apparition of spurious oscillations and smoothing effects.

The notations here are straightforwardly extended from the one of the discretization in the original variables. We again make use of a time-splitting.

- First, we solve the advection equation

$$\partial_\tau g(\tau,y) + \partial_y(W(\tau,y)g(\tau,y)) = g(\tau,y).$$

  Knowing d^n and g^n approximations of the rescaled monomers concentration d and particles distribution g at time $\tau^{(n)}$, respectively, we use the ADM scheme to determine

$$g_k^{n+1} = g_k^n - \frac{\Delta\tau^{(n)}}{\Delta y}(W_{k+1/2}^n g_{k+1/2}^n - W_{k-1/2}^n g_{k-1/2}^n) + \Delta\tau^{(n)} g_k^n.$$

  The only modification is to take into account the zeroth-order term, but it is straightforward to adapt the scheme and Proposition 3.1 to this situation.
- Finally, we update the monomers concentration with

$$d(\tau)\exp\left(-\frac{\tau}{3}\right) + \int_0^\infty y g(\tau,y)\mathrm{d}y = \rho.$$

  For the discrete unknowns, it yields

$$d^{n+1} = \left(\rho - \sum_{k=0}^{K} y_k g_k^{n+1}\Delta y\right)\exp\left((n+1)\frac{\Delta\tau}{3}\right), \quad \text{with } y_k = \left(k+\frac{1}{2}\right)\Delta y.$$

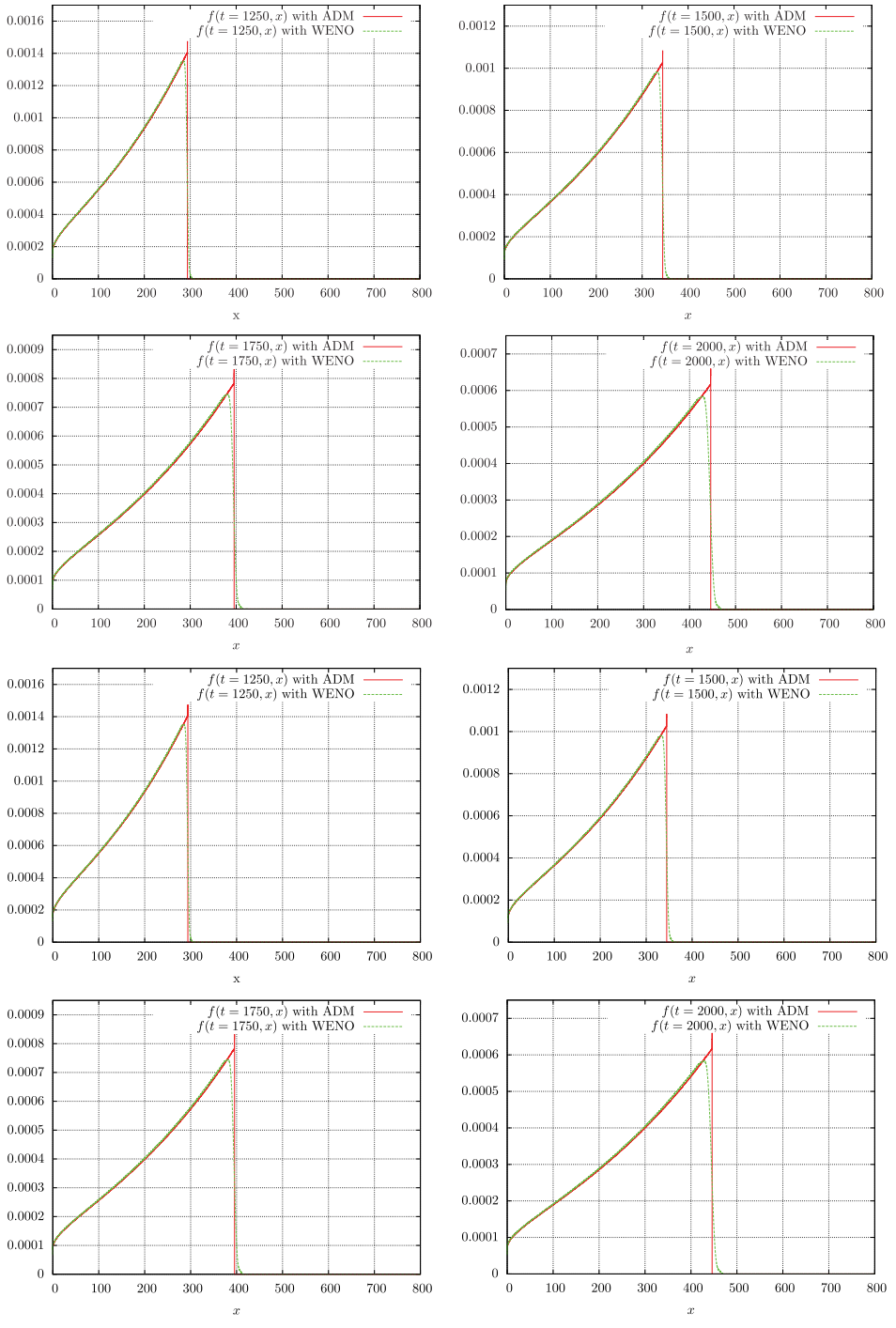

Fig. 3. Comparison WENO vs. ADM schemes. Evolution of the solution all 2.5 time units.

Using the scheme in this way we observe the apparition of spurious oscillations. In fact, in rescaled variables it seems that additional stability constraints need to be considered in the definition of the monomers concentration d. A rough derivation of a criterion that prevents the formation of oscillation works as follows. We have

$$\frac{\mathrm{d}}{\mathrm{d}\tau}d(\tau) = e^{\tau/3}\left(\frac{\rho}{3} - \frac{4}{3}\int_0^\infty yg(\tau,y)\mathrm{d}y - \int_0^\infty W(y,\tau)g(\tau,y)\mathrm{d}y\right).$$

From this relation we deduce that $\frac{\mathrm{d}}{\mathrm{d}\tau}d$ can be estimated by $\mathscr{O}(e^{\tau/3})$. By analogy with the basic theory of numerical integration of ODE, this estimate suggests to impose $\Delta\tau \leq Ce^{-\tau/3}$ as a stability criterion. Of course, as time increases this becomes much more restrictive than the CFL condition (3.4) associated to the transport equation. We are not able to propose a complete analysis, nevertheless this condition turns out to be efficient. From our numerical experiences it seems also difficult to relax it.

Again we compare the results with the ADM and WENO schemes. The data are defined as follows:

- the domain is $[0, 40]$ with 1000 points by unit length;
- the initial data is

$$\rho = 41 \quad (\text{corresponding to } d^0 = 1),$$
$$g^0(y) = \begin{cases} 0.1, & y \in [10, 30], \\ 0, & \text{otherwise.} \end{cases} \tag{3.11}$$

Results are displayed in Fig. 4 at the final time $\tau = 20$. We also show the time evolution of the particles distribution in Fig. 5. We remind, see the comments in Ref. 3, that the rescaled problem is highly stiff and sensible to numerical diffusion. The non-dissipative character of the ADM scheme is definitely an asset to capture with accuracy the correct profile. Indeed, with the chosen numerical conditions, the effects of numerical dissipation appear sensitively at time $\tau = 7.5$ with the

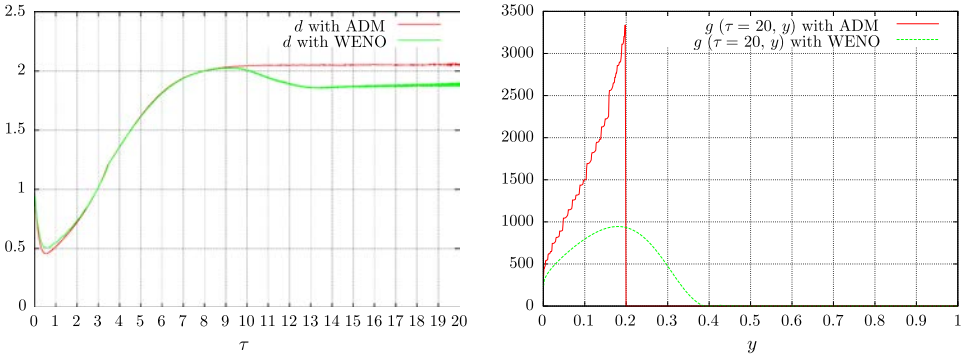

Fig. 4. Comparison of WENO and ADM on the rescaled equation, with the initial characteristic function of (3.11). *Left*: evolution of rescaled monomers concentration. *Right*: final rescaled solution.

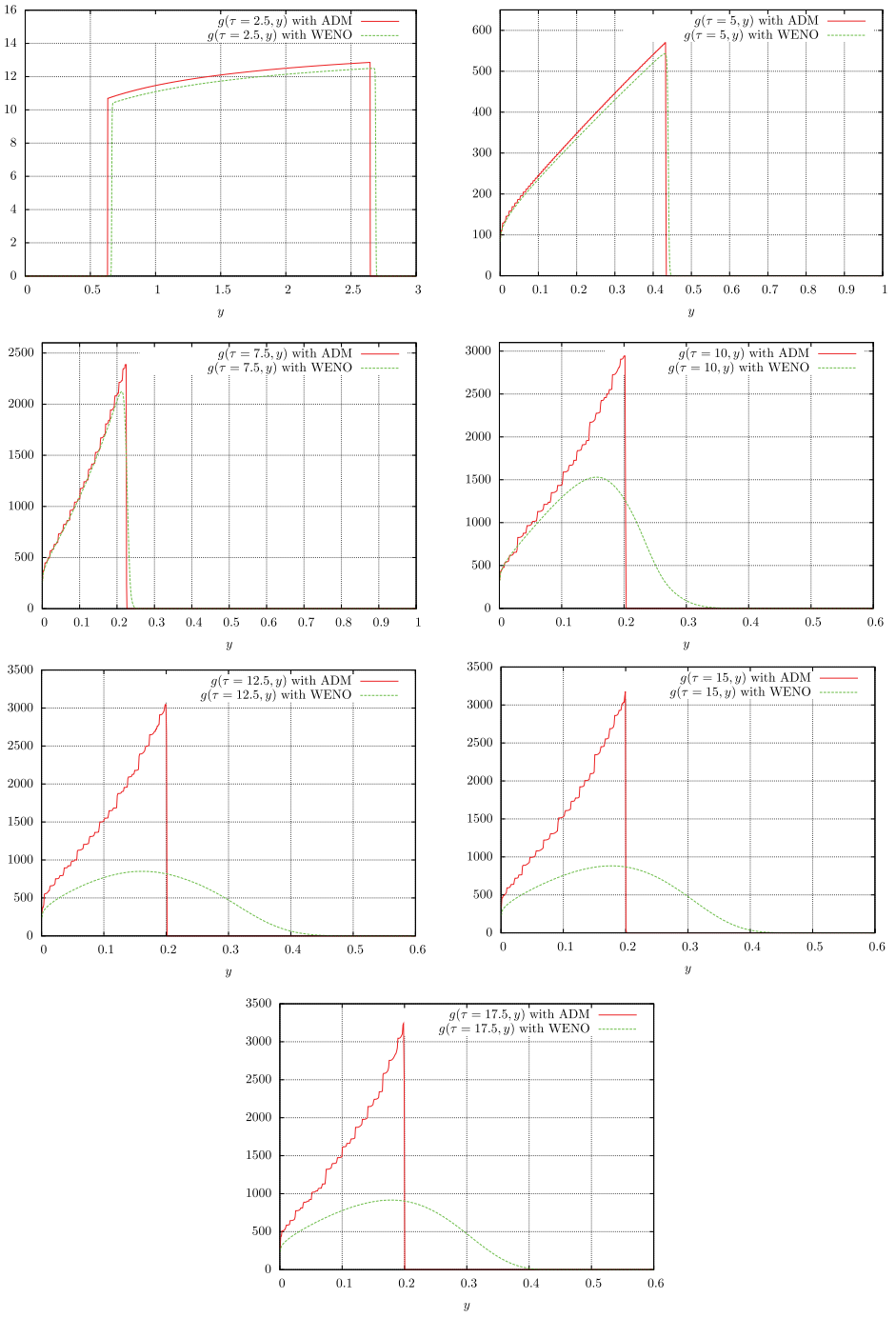

Fig. 5. Comparison WENO vs. ADM on the rescaled equation. Evolution of the rescaled solution all 2.5 time units.

WENO scheme. Since this time, the smoothing effect propagates and, continuing the simulation, the asymptotic profile we obtain looks like the smooth LS profile. (Note that we also remarked, during our experiences, that this profile is the one obtained when taking a smooth initial density, such as a Maxwellian.) This is confirmed by looking at the behavior of the monomers concentration d: the ADM method keeps d close to the expected value ($K = 2.05197$), while with WENO it decays to $K_{\mathrm{LS}} = 1.88988$.

Remark 3.1. We here (and in all the following tests) notice an already known drawback of the anti-dissipative limited downwind scheme: the staircase effect. Indeed, this scheme has the property of "projecting" any (even smooth) initial datum on the set of staircased data. This seems to appear during the very first steps of the loop. On the one hand, this is a drawback because it reduces the precision of the scheme. Nevertheless, on the other hand, it seems that the very good large time behavior of the scheme is intrically linked with the staircase effect. The scheme is indeed proven to be exact for staircased data in Ref. 11, in the case of advection with constant velocity. A precise analysis of the behavior for a smooth initial data is lacking. By the way, we *notice* here that the local staircases do not seem to have global effects on the solutions.

Furthermore, this simulation in rescaled variables goes twice faster with the ADM scheme than with the WENO scheme (using the same CFL parameter as in Ref. 3) despite the restriction imposed by the exponential stability condition.

Finally, we end the validation of the ADM scheme by imposing the analytic asymptotic profile (here with $p = 1$ see Fig. 1) as initial condition and $d(\tau) = 2.05197$. The result reported in Fig. 6 shows that the solution is well-preserved by the scheme.

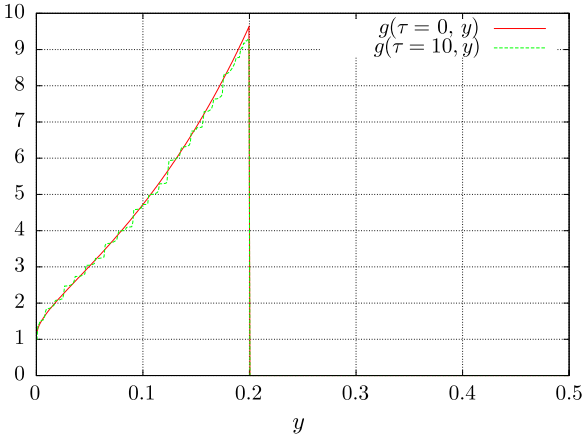

Fig. 6. ADM: behavior of the rescaled solution by starting with the analytic asymptotic profile for $p = 1$.

4. Treatment of the Coagulation Operator

In this section we wish to investigate numerically how the coagulation term $Q_{\rm coag}$ modifies the asymptotic behavior of the solutions. To this end we need to incorporate in the time-splitting algorithm the treatment of the collision term. We first propose a "naive" approach where the integral operator is evaluated directly. As we shall see the computational cost of this method is quite heavy. Therefore, we adapt the treatment of coagulation terms introduced by Filbet and Laurençot.[14] The idea is to make from $Q_{\rm coag}$ the derivative of a flux $\partial_x J$ appear, which, in turn, can be naturally treated in a Finite Volume framework.

4.1. *Direct evaluation of the coagulation term*

We remind that $Q_{\rm coag}(f) = Q^+_{\rm coag}(f) - Q^-_{\rm coag}(f)$ where

$$Q^-_{\rm coag}(f) = f \times L(f), \quad L(f) = \int_0^\infty f(t,y)\mathrm{d}y.$$

The PDE governing the size density is

$$\partial_t f + \partial_x(Vf) = \lambda Q^+_{\rm coag}(f) - f \times \lambda L(f).$$

Then, the scheme splits into the following steps:

- First, we solve the transport equation

$$\partial_t f + \partial_x(V(t,x)f) = 0.$$

  Here, we assume that the monomers concentration does not change: $c(t)$ is replaced by c^n and we make use of either the WENO or the ADM scheme. It defines $f^{n+1/2}$. We write $f_k^{n+1/2} = f_k^n - \frac{\Delta t^{(n)}}{\Delta x}(V^n_{k+1/2} f^n_{k+1/2} - V^n_{k-1/2} f^n_{k-1/2})$, and the fluxes $f^n_{k+1/2}$ are chosen according to the anti-dissipative method or the WENO scheme).
- Second, we solve

$$\partial_t f(t,x) + \lambda L(f) \times f = \lambda Q^+_{\rm coag}(f).$$

  We adopt a semi-implicit viewpoint. We rewrite this equation as

$$\frac{\mathrm{d}}{\mathrm{d}t}\left[f \exp\left(\lambda \int_0^t L(f)(s)\mathrm{d}s\right)\right] = \exp\left(\lambda \int_0^t L(f)(s)\mathrm{d}s\right) \lambda Q^+_{\rm coag}(f).$$

  We integrate over a time step, assuming that $Q^+_{\rm coag}(f)$ and $L(f)$ do not change on $(t^{(n)}, t^{(n+1)})$. We are led to the following formula

$$f_k^{n+1} = \exp(-\ell_k^{n+1/2}\Delta t^{(n)}) f_k^{n+1/2} + q_k^{n+1/2}\left(\frac{1-\exp(-\ell_k^{n+1/2}\Delta t^{(n)})}{\ell_k^{n+1/2}}\right),$$

  where $q_k^{n+1/2}$ and $\ell_k^{n+1/2}$ correspond to the discrete version of the integral operators $\lambda Q^+_{\rm coag}(f^{n+1/2})$ and $\lambda L(f^{n+1/2})$, the monomers concentration being still

determined by c^n. The advantage of such a formula is that it naturally preserves the non-negativity of the solution.

- We update the monomers concentration with

$$c(t) + \int_0^\infty x f(t,x)\mathrm{d}x = \rho.$$

We thus set

$$c^{n+1} = \rho - \Delta x \sum_{k\in\mathbb{N}} x_k f_k^{n+1}.$$

For the simulations, the data are given as follows:

- the domain $[0, 2200]$ with 20 points by unit length;
- the initial function is

$$f^0(x) = \begin{cases} 0.1, & x \in [10,30], \\ 0, & \text{otherwise;} \end{cases} \tag{4.1}$$

- the total initial mass is $\rho = 41$ so that the initial monomers concentration is $c^0 = 1$.

We show in Figs. 7 and 8 a comparison between the ADM and fifth-order WENO schemes ("asymptotic" profiles at the final time $t = 800$, and pictures of the evolution of the particles concentration each 75 time units). Here we have set $\lambda = 1/100$. We observe a remarkable agreement between the two methods. However, the ADM run is faster by a factor 2. Then we do not observe any numerical interference between the discretization of the transport term and the treatment of the coagulation term. Since the ADM scheme has better performances, we shall use it for further simulations.

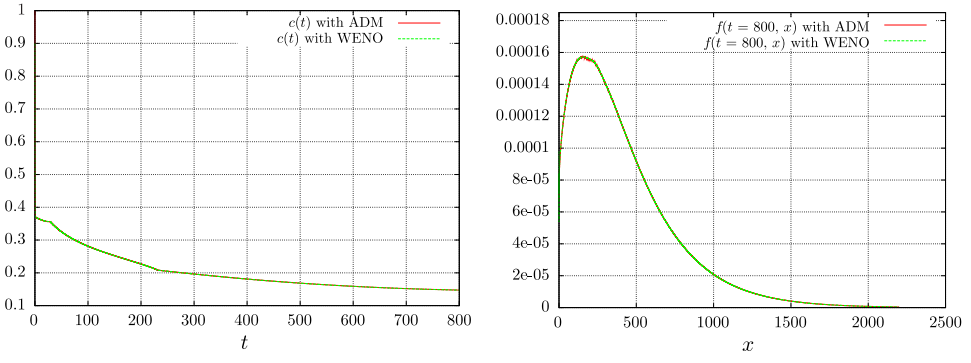

Fig. 7. Comparison of WENO and ADM on the equation with encounters, with the characteristic initial condition of (3.10). *Left*: evolution of monomers concentration. *Right*: final solution at time $t = 800$ with $\lambda = 1/100$.

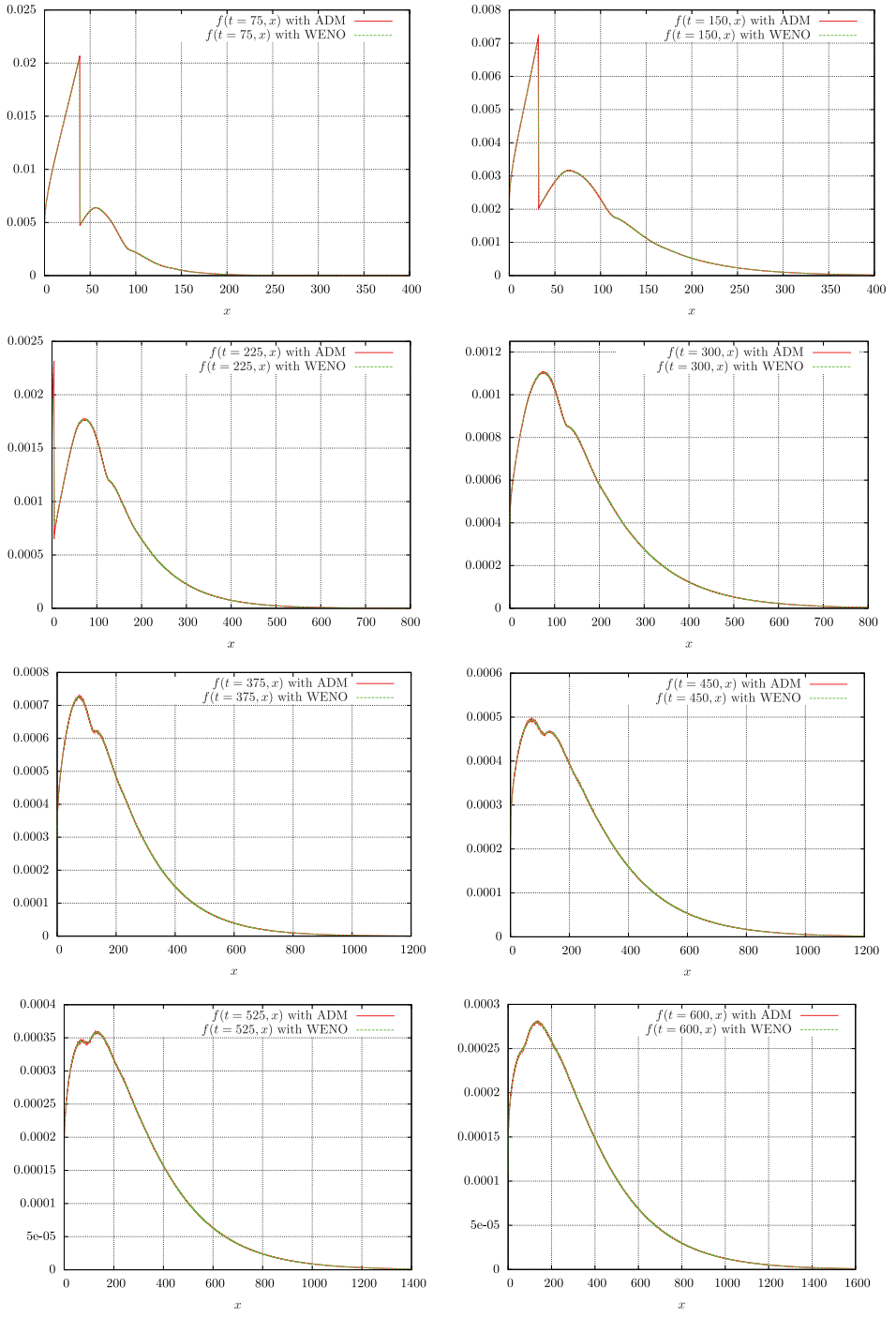

Fig. 8. Comparison WENO vs. ADM on the equation with encounters. Evolution of the solution all 75 time units with $\lambda = 1/100$.

Next, we compare the evolution when we start from different initial data: we consider the step function and the following Maxwellian distribution:

$$f^0(x) = \frac{4}{\sqrt{2\pi}} \exp\left(-\frac{(x-10)^2}{2}\right). \tag{4.2}$$

All the other parameters are kept the same, and we work with the ADM scheme. Results are displayed in Fig. 9. The noticeable point is that now the shapes of the solutions look equally smooth after 800 time units. Comparing the time evolution in Fig. 8 (step function) we can see that the regularizing effects come from the largest particles and propagate to smooth out the front.

Finally, we make the parameter λ vary: as it increases, the influence of the coagulation is more important. As λ becomes close to 1 we need an extended computational domain to keep accurate simulations: indeed, due to the convolution operator, the support of the solution spreads out and larger particles have to be considered as λ increases. For example with $\lambda = 1/10$ we work with the domain $[0, 6000]$ and 10 points by unit length, see Figs. 10–13. The rate of convergence towards the asymptotic profile seems to be highly dependent on the coefficient λ: the larger λ, the faster the convergence.

Simulation of the model with encounters in rescaled variables. We switch to the system (2.1) written in rescaled coordinates. Hence, the time-splitting adapts as follows:

- First, we solve

$$\partial_\tau g + \partial_y(Wg) = g,$$

with fixed monomers concentration d^n. We use the ADM scheme and it defines $g^{n+1/2}$ as follows:

$$g_k^{n+1/2} = (1 + \Delta\tau^{(n)})g_k^n - \frac{\Delta\tau^{(n)}}{\Delta x}(W_{k+1/2}^n g_{k+1/2}^n - W_{k-1/2}^n g_{k-1/2}^n).$$

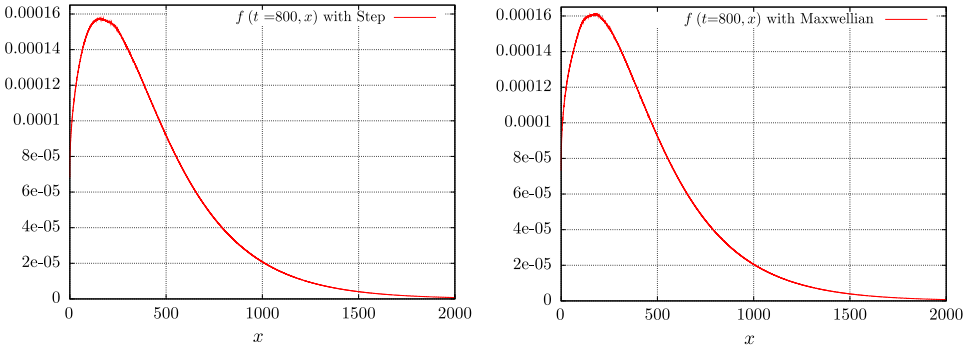

Fig. 9. ADM scheme for the equation with encounters for $\lambda = 1/100$. *Left*: with the characteristic function initial condition (3.10). *Right*: with the Maxwellian initial condition (4.2), and $\rho = 41$, too.

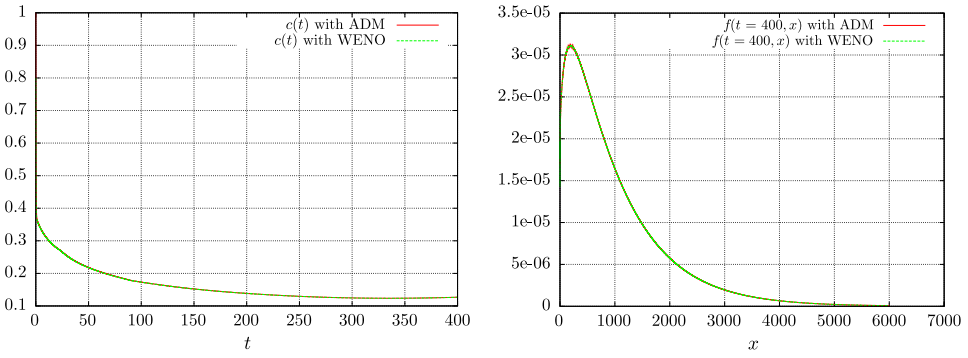

Fig. 10. Comparison of WENO and ADM on the equation with encounters, with the characteristic function (3.10) as initial condition. *Left*: evolution of monomers concentration. *Right*: final solution at time $t = 400$ with $\lambda = 1/10$.

- Second, we consider the collision terms which leads to consider the following ODE:

$$\partial_\tau g(\tau, y) + \lambda L^r(g) g(\tau, y) = \lambda Q^{r+}_{\text{coag}}(g)(\tau, y),$$

where

$$L^r(g) = \int_0^\infty g(y)\mathrm{d}y \quad \text{and} \quad Q^{r+}_{\text{coag}}(g) = \frac{1}{2}\int_0^y g(y-u)g(u)\mathrm{d}u.$$

We adopt a semi-implicit viewpoint to solve

$$\partial_\tau g(\tau, y) + \ell^r g = q^r,$$

or, in other words, we set

$$g_k^{n+1} = g_k^{n+1/2}\exp(-\ell_k^{r,n+1/2}\Delta\tau^{(n)}) + q_k^{r,n+1/2}\left(\frac{1-\exp(-\ell_k^{r,n+1/2})\Delta\tau^{(n)})}{\ell_k^{r,n+1/2}}\right),$$

where $q_k^{r,n+1/2}$ and $\ell_k^{r,n+1/2}$ correspond to the approximation of $\lambda Q^{r+}_{\text{coag}}(g)$ and $\lambda L^r(g)$, respectively, defined with $g^{n+1/2}$ and d^n.

- Finally, we use the mass constraint

$$d(\tau)\exp\left(-\frac{\tau}{3}\right) + \int_0^\infty y g(\tau, y)\mathrm{d}y = \rho,$$

which yields

$$d^{n+1} = \left(\rho - \sum_{k=0}^{K} y_k g_k^{n+1}\Delta y\right)\exp\left(\frac{(n+1)\Delta t^{(n)}}{3}\right).$$

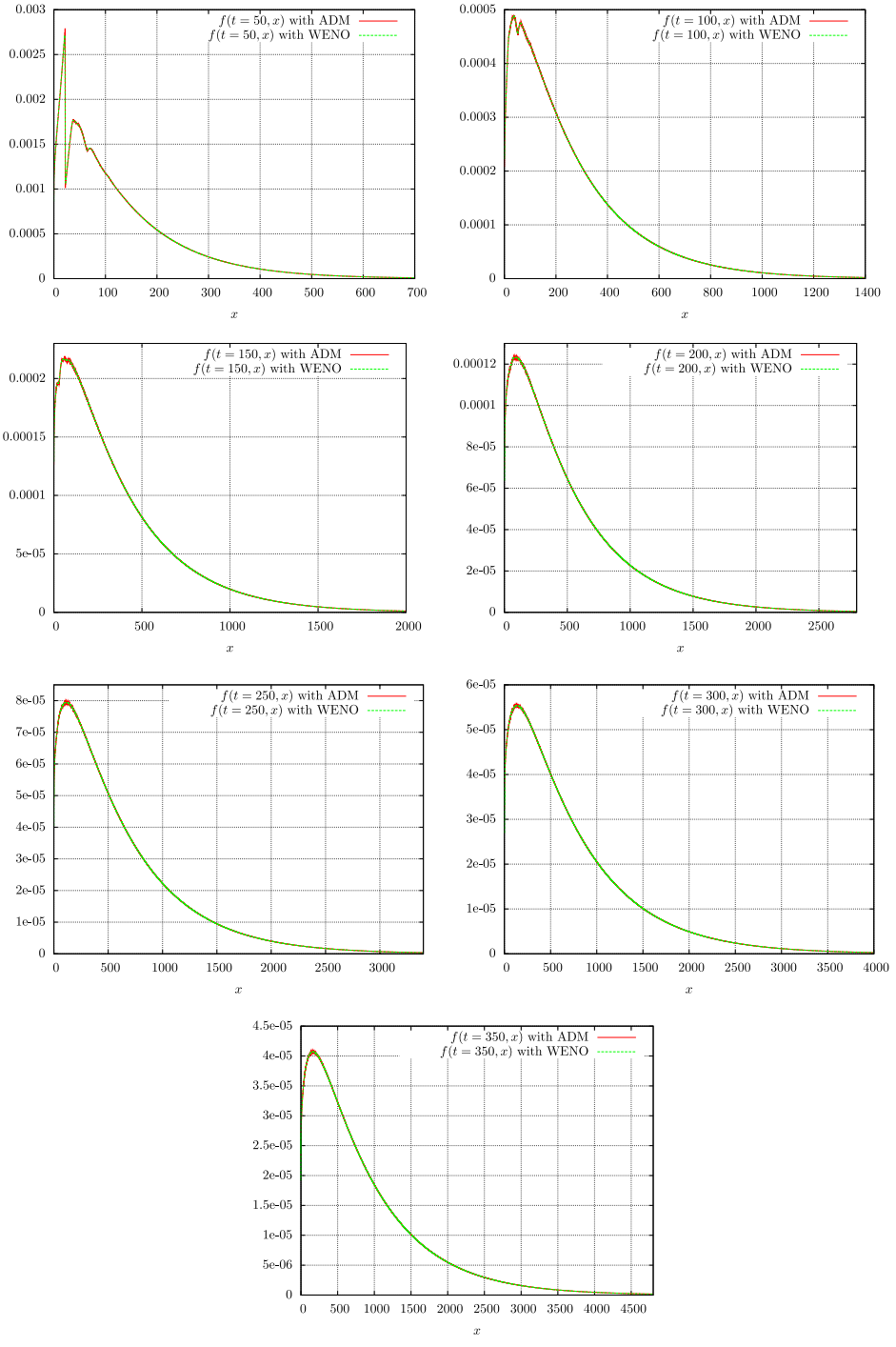

Fig. 11. Comparison WENO vs. ADM on the equation with encounters. Evolution of the solution all 50 time units with $\lambda = 1/10$.

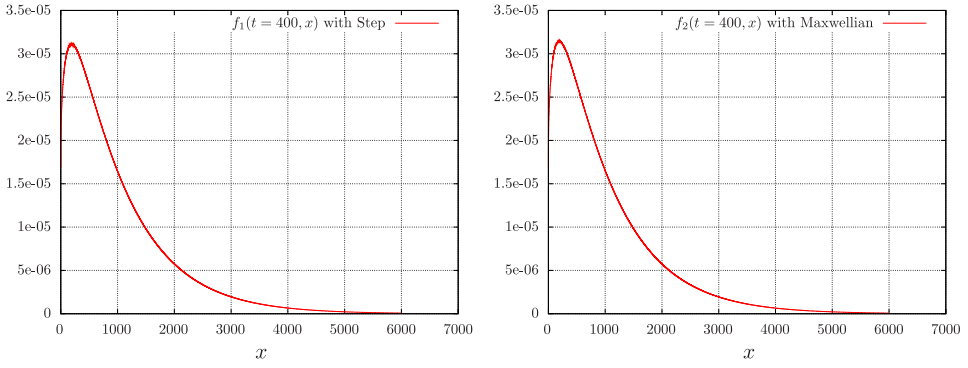

Fig. 12. ADM scheme for the equation with encounters for $\lambda = 1/10$. *Left*: characteristic initial condition (3.10). *Right*: Maxwellian initial function (4.2).

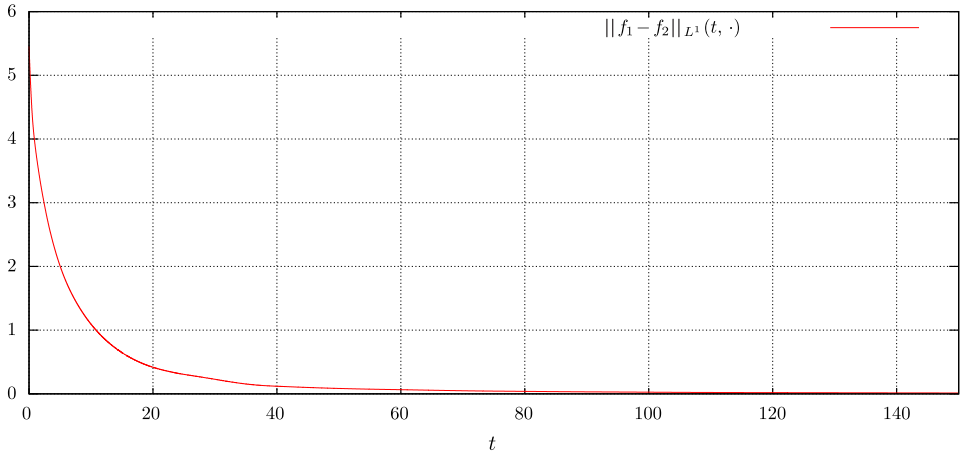

Fig. 13. Relaxation velocity: L^1-norm of the time evolution of the two solutions f_1 and f_2. It behaves like $5.13\exp(-\frac{t^{3/4}}{4})$.

We perform the simulation of the rescaled equation with encounters considering the following data:

- We bear in mind that considering the coagulation terms, we lose the support property of the solution in rescaled variables. Indeed, Q^+ and L are integral operators and they act like a convolution so that the support of the stationary solution is expected to fill the whole line $y \geq 0$: the main part of the information is likely contained in a bounded domain but the effect of the tail can be important, see Refs. 25 and 17. Accordingly, the definition of the computational domain is very sensitive, as already shown in original variables, to the value of the parameter λ. Then we choose the domain $[0, 100]$ with 200 points by unit length for $\lambda = 1/100$ and for $\lambda = 1/10$ we choose the domain $[0, 150]$ with 200 points by unit length.

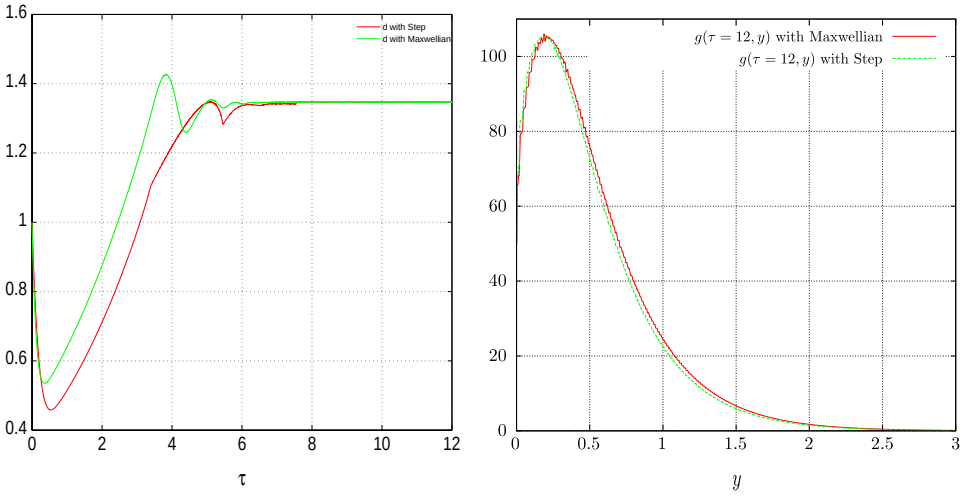

Fig. 14. ADM scheme for the equation with encounters for $\lambda = 1/100$. *Left*: characteristic initial function (3.10). *Right*: Maxwellian initial function g^0 defined as (4.2).

- The total initial mass $\rho = 41$ is chosen so that the initial monomers concentration is $d^0 = 1$.

In Fig. 14 we compare the solutions associated to a Maxwellian initial data or a step function with $\lambda = 1/100$. Of course the remarkable fact is that $d(\tau)$ tends to the same constant, which however differs from $K_{\mathrm{LS}} \simeq 1.88988$, while the solutions have a very similar profile at $\tau = 12$. We can expect that the stationary solution has an infinite support and we indeed observe that large particles should be considered compared to the compactly supported profiles of the collisionless equation. We see on Figs. 14 and 15 the time evolution of the particles distributions, where we can observe the regularizing effects due to the collision term and the spreading of the support. All these effects appear similarly when we make λ vary, see, for instance, Fig. 15. We remark that the asymptotic value of d depends on λ. However our numerical investigation shows that letting λ go to 0, the large time value of $d(\tau)$ tends to K_{LS}.

4.2. (*Conservative*) *Finite volume approximation of the coagulation term*

In this section we propose another method to evaluate the coagulation operator, inspired from Ref. 14. Let us remind how the scheme of Filbet and Laurençot[14] works when dealing with

$$\partial_t f = \lambda Q_{\mathrm{coag}}(f).$$

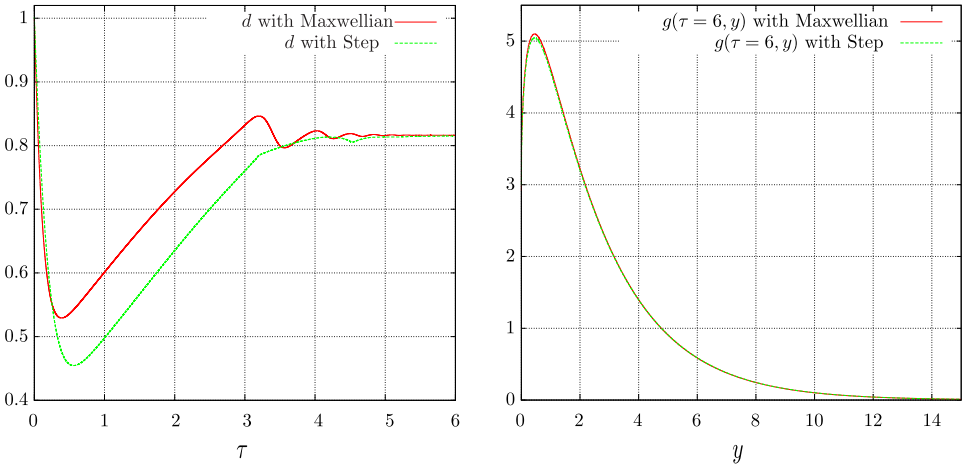

Fig. 15. ADM scheme for the equation with encounters for $\lambda = 1/10$. *Left*: characteristic initial condition. *Right*: Maxwellian initial condition.

The starting point of the method consists in rewriting the problem as follows:

$$x\partial_t f(t,x) = \lambda x Q_{\text{coag}}(f)(t,x) = -\lambda \partial_x J(f),$$

where

$$J(f)(t,x) = \int_0^x \int_{x-u}^{\infty} u f(t,u) f(t,v) \mathrm{d}v \mathrm{d}u.$$

The next step relies on the approximation of the integrals that define $J(f)$ and the necessary truncation, embodied into a parameter $0 < R < \infty$, of the infinite integration domain. In Ref. 14 two approaches are designed:

- The "conservative method", which consists in replacing $J(f)$ by

$$J^R_{\text{coag}}(f)(t,x) = \int_0^x \int_{x-u}^{R-u} u f(t,u) f(t,v) \mathrm{d}v \mathrm{d}u$$

for $0 < x < R < \infty$. We remark that $J^R_{\text{coag}}(f)(t,R) = J^R_{\text{coag}}(f)(t,0) = 0$. Consequently, the solution f_R of

$$x\partial_t f_R(t,x) = -\lambda \partial_x J^R_{\text{coag}}(f_R), \quad t \geq 0, \quad 0 \leq x \leq R < \infty,$$

satisfies the preservation of the first-order moment:

$$\int_0^R x f_R(t,x) \mathrm{d}x = \int_0^R x f_R(0,x) \mathrm{d}x.$$

- The "non-conservative method" where we set

$$J_{nc}^R(f)(t,x) = \int_0^x \int_{x-u}^R u f(t,u) f(t,v) \mathrm{d}v \mathrm{d}u$$

for $0 < x < R < \infty$. Again, we have

$$x \partial_t f_R(t,x) = -\lambda \partial_x J_{nc}^R(f_R),$$

but now the first moment of f_R is non-increasing.

We refer to Ref. 14 for a thorough analysis of the method and in particular for convergence analysis as $R \to \infty$, which typically holds under sublinear growth assumption on the coagulation kernel (see also Refs. 12 and 39). The problem addressed in Ref. 14 is essentially concerned with the capture of the gelation phenomenon, that is a loss of mass in finite time, a typical feature of certain coagulation equations. Here, the situation is different and it turns out that the conservation of the first moment by the encounters process is crucial for the accuracy of the scheme and the evaluation of the monomers concentration in the last step of the splitting. For this reason, we work here with the conservative method.

To obtain the discrete expression of the operator J_{coag}^R it is convenient to introduce the change of variables $w = u + v$ so that J_{coag}^R recasts as

$$J_{\mathrm{coag}}^R(f)(t,x) = \int_0^x \int_x^R u f(t,u) f(t,w-u) \mathrm{d}w \mathrm{d}u.$$

Recall that $x_k = (k+1/2)\Delta x$, for $k \in \{0, \dots, k_M - 1\}$ where $k_M = R/\Delta x$ is the number of cells. We use the following approximation

$$J_{\mathrm{coag}}^R(f)_{k+1/2}^n = \sum_{j=0}^{k} \sum_{l=k}^{K} x_j f_j^n f_{l-j}^n \Delta x^2 \tag{4.3}$$

with the boundary condition $J_{\mathrm{coag}}^R(f)_{1/2}^n = J_{\mathrm{coag}}^R(f)_{k_M-1/2}^n = 0$. Then, the time-splitting is organized as follows:

- First, we solve on a time step

$$\partial_t f + \partial_x(Vf) = 0.$$

To this end, we make use of the ADM scheme by assuming that the monomers concentration does not change: $c(t)$ is replaced by c^n. It defines $f_k^{n+1/2}$ as follows:

$$f_k^{n+1/2} = f_k^n - \frac{\Delta t^{(n)}}{\Delta x}(V_{k+1/2}^n f_{k+1/2}^n - V_{k-1/2}^n f_{k-1/2}^n).$$

- Second, we solve

$$\partial_t(xf) = -\lambda \partial_x J_{\mathrm{coag}}^R(f).$$

We are led to the following formula:

$$x_k f_k^{n+1} = x_k f_k^{n+1/2} - \lambda \frac{\Delta t^{(n)}}{\Delta x}(J_{k+1/2}^{n+1/2} - J_{k-1/2}^{n+1/2}),$$

where the numerical flux $J_{k+1/2}^n$ is the approximation $J_{\text{coag}}^R(f)_{k+1/2}^n$.

- We update the monomers concentration by $c^{n+1} = \rho - \sum_{k=0}^K x_k f_k^{n+1} \Delta x$.

We consider the same data as when dealing with the naive approach for the problem with coagulation in original variables. It allows to compare the two methods. The decisive advantage for the conservative Finite Volume approximation of the coagulation term relies on the fact that it does not need a very large computational domain. In turn, the computation is definitely less costly.

The numerical results obtained with the Filbet–Laurençot approach in Figs. 16 and 17 are very close to the corresponding results based on the "naive" approach in Figs. 7 and 8. The numerical results show again the regularizing effect of the encounters in the asymptotic behavior of the model. For instance, Figs. 18 and 19 compare the solutions starting from the step and the Maxwellian initial data, as in Figs. 9 and 10.

Numerical study in rescaled variables with coagulation operator in conservative form. In rescaled variables the system reads

$$\begin{cases} \partial_\tau g + \partial_y(Wg) = g(\tau, y) + \lambda Q_{\text{coag}}^r(g), \quad \tau \geq 0, \ \ y \geq 0, \\ d(\tau) \exp\left(-\dfrac{\tau}{3}\right) + \displaystyle\int_0^\infty y g(\tau, y) \mathrm{d}y = \rho, \quad \tau \geq 0, \\ g(0, y) = g^0(y), \quad y \geq 0, \quad W(\tau, y) = y^{1/3} d(\tau) - 1 - y, \quad \tau \geq 0, \ \ y \geq 0, \end{cases}$$

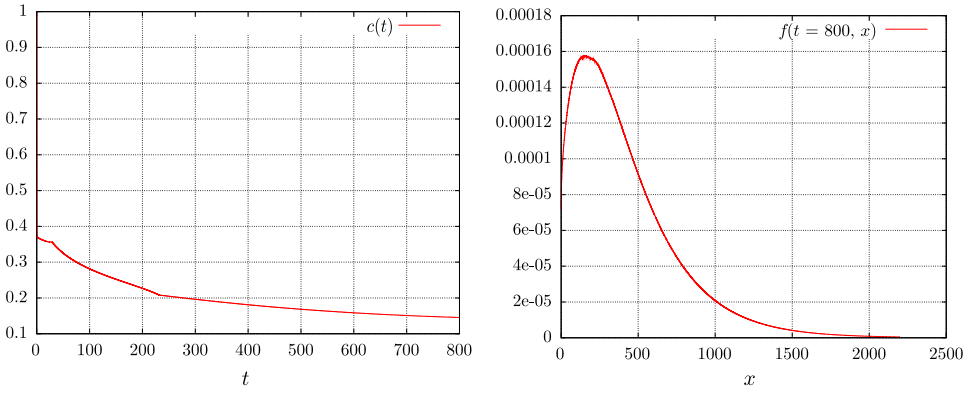

Fig. 16. ADM+Filbet–Laurençot approach for encounters with $\lambda = 1/100$, with the characteristic function as initial condition. *Left*: evolution of monomers concentration. *Right*: final solution at time $t = 800$.

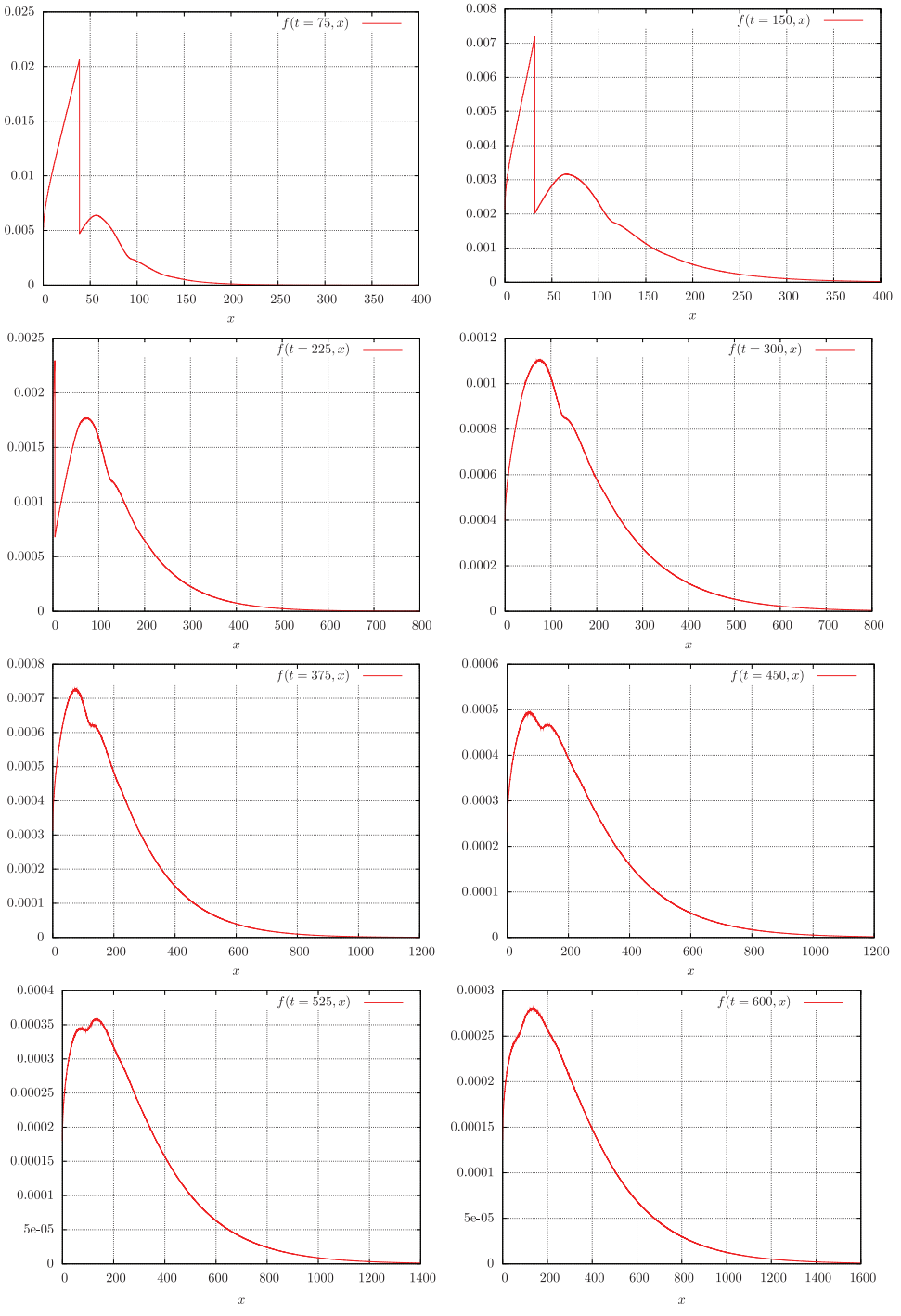

Fig. 17. ADM+Filbet–Laurençot approach for encounters with $\lambda = 1/100$. Evolution of the solution all 75 time units.

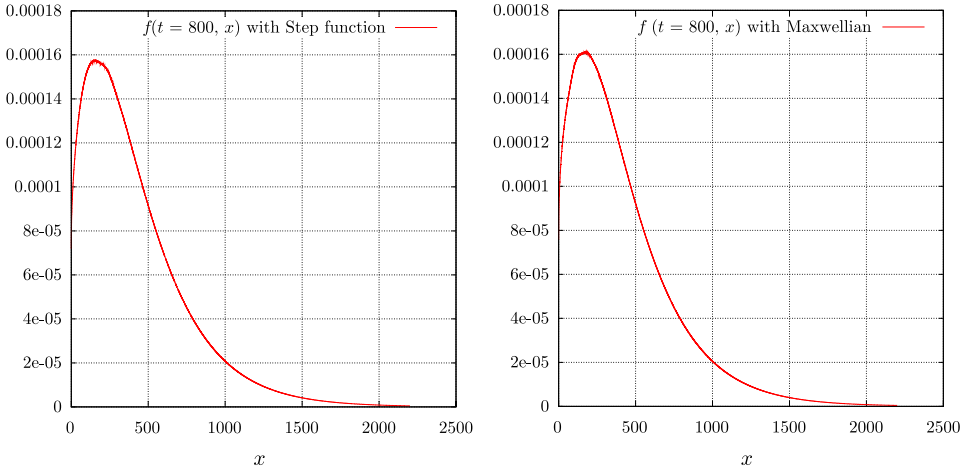

Fig. 18. ADM+Filbet–Laurençot approach for encounters with $\lambda = 1/100$. *Left*: characteristic initial condition. *Right*: Maxwellian initial condition.

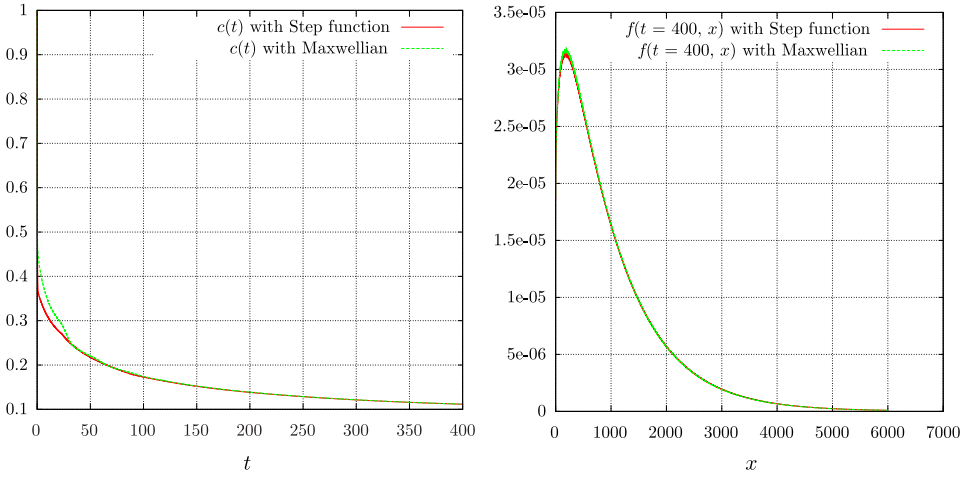

Fig. 19. ADM+Filbet–Laurençot approach for encounters with $\lambda = 10$, for both the characteristic and the Maxwellian initial conditions. *Left*: evolution of monomers concentration. *Right*: final solution at time $t = 400$.

where ρ is a constant. We proceed as previously with the following time-splitting:

- $\partial_\tau g + \partial_y(Wg) = g(\tau, y)$;
- $\partial_\tau g = \lambda Q^r_{\text{coag}}(g)$.

The fundamental point consists in transforming this last equation in the conservative flux form as above. As it is straightforward, we omit the details.

Simulation in rescaled variables with coagulation operator in conservative form. The data are defined as follows:

- The length domain is $[0, 40]$ with 1000 points by unit length which means $\Delta x = 4 \cdot 10^{-2}$.
- The initial function is

$$g^0(x) = \begin{cases} 0.1, & x \in [10, 30], \\ 0, & x > 30. \end{cases}$$

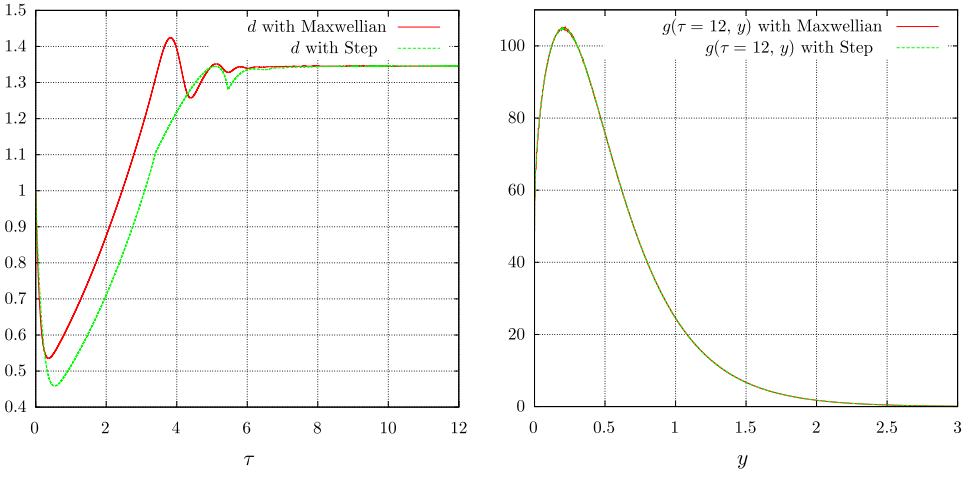

Fig. 20. ADM+Filbet–Laurençot approach for encounters in rescaled variables with $\lambda = 1/100$. *Left*: characteristic initial condition. *Right*: Maxwellian initial condition.

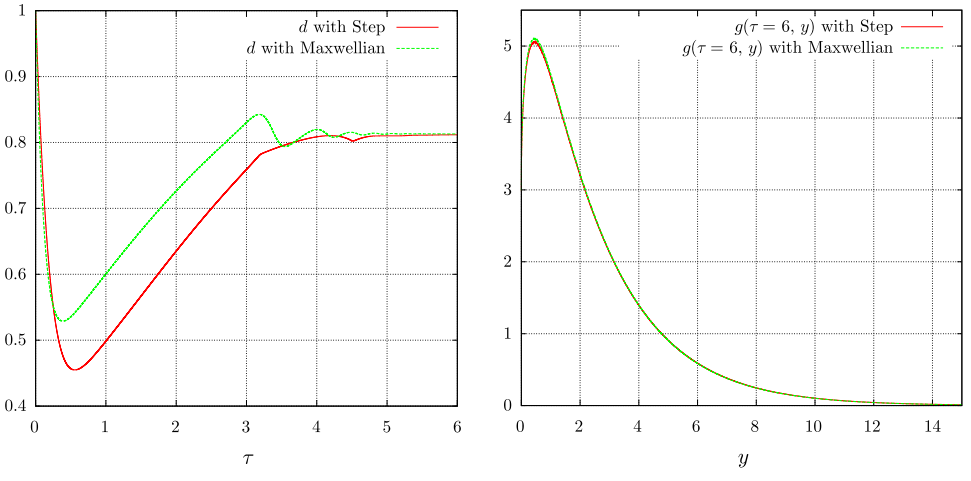

Fig. 21. ADM+Filbet–Laurençot approach for encounters in rescaled variables with $\lambda = 1/10$. *Left*: characteristic initial condition. *Right*: Maxwellian initial condition.

- The total initial mass $\rho = 41$ is chosen so that the initial monomers rescaled concentration is $d^0 = 1$.

Results are displayed in Fig. 20 for the parameter $\lambda = 1/100$ and in Fig. 21 for $\lambda = 1/10$.

The results confirm what has been said above. Using the conservative approach for the coagulation term allows to keep a reduced computational domain, and thus preserves the computational cost. The effect of the coagulation term is again to smooth out the profile.

5. Conclusion

We discuss on numerical grounds several aspects of the Lifshitz–Slyozov system. To this end, we introduce a new scheme for the collisionless model: based on anti-diffusive strategies, the scheme captures the singular profiles exhibited by the system in large times, and it outperforms other methods used to address the problem. Next, we investigate the effects of the addition of a coagulation term in the equation. Results should be considered cautiously and they have a purely experimental status but the preliminary study indicates that the coagulation operator can have a regularizing effect, which in turn can dictate the selection of the smooth profile predicted by Lifshitz–Slyozov. We wish this work will be a source of inspiration for further analysis of this challenging problem.

Acknowledgment

We thank J. A. Carrillo for many advices on the WENO code used in Ref. 3. We are also gratefully indebted to P. Lafitte who pointed to our attention Ref. 14 and for warm and constant encouragements.

References

1. L. Brown, A new examination of classical coarsening theory, *Acta Metall.* **37** (1989) 71–77.
2. J. Carr and O. Penrose, Asymptotic behavior of solutions to a simplified Lifshitz–Slyozov equation, *Physica D* **124** (1998) 166–176.
3. J. A. Carrillo and T. Goudon, A numerical study on large-time asymptotics of the Lifshitz–Slyozov system, *J. Sci. Comput.* **18** (2003) 429–473.
4. M. K. Chen and P. W. Voorhees, The dynamics of transient Ostwald ripening, *Modelling Simulat. Mater. Sci. Engrg.* **1** (1993) 591–612.
5. J.-F. Collet and T. Goudon, Lifshitz–Slyozov equations: The model with encounters, *Transp. Theory Stat. Phys.* **28** (1999) 545–573.
6. J.-F. Collet and T. Goudon, On solutions of the Lifshitz–Slyozov model, *Nonlinearity* **13** (2000) 1239–1262.
7. J.-F. Collet, T. Goudon, F. Poupaud and A. Vasseur, The Becker–Döring system and its Lifshitz–Slyozov limit, *SIAM J. Appl. Math.* **62** (2002) 1488–1500.
8. J.-F. Collet, T. Goudon and A. Vasseur, Some remarks on large-time asymptotics of the Lifshitz–Slyozov equations, *J. Stat. Phys.* **108** (2002) 341–359.

9. J. Conlon, On a diffusive version of the Lifshitz–Slyozov–Wagner equation, *J. Nonlinear Sci.* **20** (2010) 463–521.
10. D. B. Dadyburjor and E. Ruckenstein, Kinetics of Ostwald ripening, *J. Crystal Growth* **40** (1977) 279–290.
11. B. Després and F. Lagoutière, Contact discontinuity capturing schemes for linear advection and compressible gas dynamics, *J. Sci. Comput.* **16** (2001) 479–524.
12. P. B. Dubovskii and I. W. Stewart, Existence, uniqueness and mass conservation for the coagulation–fragmentation equation, *Math. Models Methods Appl. Sci.* **19** (1996) 571–591.
13. F. Filbet and P. Laurençot, Numerical approximation of the Lifshitz–Slyozov–Wagner equation, *SIAM J. Numer. Anal.* **41** (2003) 563–588.
14. F. Filbet and P. Laurençot, Numerical simulation of the Smoluchowski coagulation equation, *SIAM J. Sci. Comput.* **25** (2004) 2004–2028.
15. S. Hariz and J.-F. Collet, A modified version of the Lifshitz–Slyozov model, *Appl. Math. Lett.* **12** (1999) 81–85.
16. A. Harten, On a class of high resolution total-variation-stable finite difference schemes, *SIAM J. Numer. Anal.* **21** (1984) 1–23.
17. M. Herrmann, B. Niethammer and J. J. L. Velázquez, Self-similar solutions for the LSW model with encounters, *J. Differential Equations* **247** (2009) 2282–2309.
18. G. Jiang and C. W. Shu, Efficient implementation of weighted ENO schemes, *J. Comput. Phys.* **126** (1996) 202–228.
19. L. Landau, E. M. Lifshitz and L. Pitaevski, *Cinétique Physique*, Coll. Physique Théorique, Vol. 10 (Mir., 1990).
20. P. Laurençot, Weak solutions to the Lifshitz–Slyozov–Wagner equation, *Indiana Univ. Math. J.* **50** (2001) 1319–1346.
21. P. Laurençot, The Lifshitz–Slyozov equation with encounters, *Math. Models Methods Appl. Sci.* **11** (2001) 731–748.
22. P. Laurençot, The Lifshitz–Slyozov–Wagner equation with conserved total volume, *SIAM J. Math. Anal.* **34** (2003) 257–272.
23. P. Laurençot and S. Mischler, From the Becker–Doring to the Lifshitz–Slyozov–Wagner equations, *J. Stat. Phys.* **106** (2002) 957–991.
24. A.-Y. Le Roux, A numerical conception of entropy for quasi-linear equations, *Math. Comput.* **31** (1977) 848–872.
25. E. M. Lifshitz and V. V. Slyozov, The kinetics of precipitation from supersaturated solid solutions, *J. Phys. Chem. Solids* **19** (1961) 35–50.
26. B. Meerson and P. Sasorov, Domain stability, competition, growth, and selection in globally constrained bistable systems, *Phys. Rev. E* **53** (1996) 3491–3494.
27. B. Niethammer, A scaling limit of the Becker–Döring equations in the regime of small excess density, *J. Nonlinear Sci.* **14** (2004) 453–468.
28. B. Niethammer and F. Otto, Ostwald ripening: The screening length revisited, *Calc. Var. Partial Differential Equations* **13** (2001) 33–68.
29. B. Niethammer and R. Pego, Non-self-similar behavior in the LSW theory of Ostwald ripening, *J. Stat. Phys.* **95** (1999) 867–902.
30. B. Niethammer and R. Pego, On the initial-value problem in the Lifshitz–Slyozov–Wagner theory of Ostwald ripening, *SIAM J. Math. Anal.* **31** (2000) 467–485.
31. B. Niethammer and R. Pego, The LSW model for domain coarsening: Asymptotic behavior for conserved total mass, *J. Stat. Phys.* **104** (2001) 1113–1144.
32. B. Niethammer and R. L. Pego, Well-posedness for measure transport in a family of nonlocal domain coarsening models, *Indiana Univ. Math. J.* **54** (2005) 499–530.

33. B. Niethammer and J. J. L. Velázquez, On the convergence to the smooth self-similar solution in the LSW model, *Indiana Univ. Math. J.* **55** (2006) 761–794.
34. B. Niethammer and J. J. L. Velázquez, On screening induced fluctuations in Ostwald ripening, *J. Stat. Phys.* **130** (2008) 415–453.
35. O. Penrose, The Becker–Döring equations at large times and their connection with the LSW theory of coarsening, *J. Stat. Phys.* **89** (1997) 305–320.
36. T. Phillips, Trouble with Lifshitz, Slyozov and Wagner, Science News, NASA Science http://www.nasa.gov/vision/earth/technologies/coarsening_prt.htm (2003).
37. V. V. Sagalovich and V. V. Slyozov, Diffusive decomposition of solid solutions, *Soviet. Phys. Usp.* **30** (1987) 23–44.
38. C. W. Shu, Essentially non-oscillatory and weighted essentially non-oscillatory schemes for hyperbolic conservation laws, in *Advanced Numerical Approximation of Nonlinear Hyperbolic Equations*, eds. B. Cockburn, C. Johnson, C. W. Shu and E. Tadmor, Lecture Notes in Mathematics, Vol. 1697 (Springer, 1998), pp. 325–432.
39. I. W. Stewart, A global existence theorem for the general coagulation–fragmentation equation with unbounded kernels, *Math. Methods Appl. Sci.* **11** (1989) 627–648.